



BUDAPEST UNIVERSITY OF TECHNOLOGY AND ECONOMICS
INSTITUTE OF NUCLEAR TECHNIQUES



CHALMERS

CHALMERS UNIVERSITY OF TECHNOLOGY
DIVISION OF SUBATOMIC, HIGH ENERGY AND PLASMA PHYSICS

BME-NTI-972/2021 | CTH-NT-345

Computational Investigation and Experimental Verification of Multiplicity Counting from the Continuous Signals of Fission Chambers

version 1.0

Authors:

Lajos Nagy, assistant researcher, BME NTI
Gergely Klujber, assistant researcher, BME NTI
Tsuyoshi Misawa, professor, Kyoto University
Yasunori Kitamura, associate professor, Kyoto University
István Barth, electrician, BME NTI
Imre Pázsit, professor, Chalmers University of Technology
Máté Szieberth, associate professor, BME NTI

Reviewed by:

Dávid Légrády, associate professor

Approved by:

Szabolcs Czifrus, director

The content of this report is the common intellectual property of the authoring institutions. Any unauthorized use is forbidden! Statements and conclusions included in this report are valid only under the conditions specified in the report.

Budapest, 10th October 2021

Document description

Document type	Research report
Document title	Computational Investigation and Experimental Verification of Multiplicity Counting from the Continuous Signals of Fission Chambers
Document registry number at BME NTI	BME-NTI-972/2021
Version number	1.0
Archived at	NTI archives
File name	bme-nti-972-2021.zip
Number of chapters	6
Number of pages	40
Number of figures	21
Number of tables	12
Content of the attached CD	-
Contract details	-
Procurer	-
Contractor	-
Contract registry number at Procurer	-
Contract registry number at Contractor	-
Date of proposal	-
Date of signature	-
Deadline	-
Assigned representative of Contractor	-
Assigned representative of Procurer	-

	Name		Signature	Date
Written by	Lajos Nagy	assistant researcher, BME NTI		
	Gergely Klujber	assistant researcher, BME NTI		
	Tsuyoshi Misawa	professor, Kyoto Univer- sity		
	Yasunori Kitamura	associate professor, Ky- oto University		
	István Barth	electrician, BME NTI		
	Imre Pázsit	professor, Chalmers Uni- versity of Technology		
	Máté Szieberth	associate professor, BME NTI		
Reviewed by	Dávid Légrády	associate professor		
Approved by	Szabolcs Czifrus	director		

Abstract

In a series of previous publications, we suggested an alternative method to the pulse-counting based multiplicity counting technique for the characterisation of special nuclear materials [1, 2, 3]. The new method uses the continuous signals of fission chambers, and the multiplicity rates, i.e. the singles, doubles and triples rates are extracted from the auto- and cross-covariances of one or more fission chambers.

Until recently only the theory of the method was elaborated. The purpose of the work described in this report was to verify the method and investigate its performance and applicability through detailed simulations as well as with a dedicated experiment. Numerical simulations of the method were performed by a code specially developed for this study, and pilot measurements were performed at the critical assembly KUCA of the Institute for Integrated Radiation and Nuclear Science, Kyoto University (KURNS). This report gives an account of both the work performed and the results of the study.

Contents

1	Introduction	2
2	Theory of multiplicity counting	4
2.1	The emission of neutrons – the superfission concept	4
2.2	Traditional multiplicity counting	6
2.3	Multiplicity counting from continuous signals	6
3	Computational tools for simulating and analysing continuous signals	9
3.1	The digital representation of signals	9
3.2	The simulation of signals	10
3.3	The analysis of signals	12
3.4	Verification of the simulation tools	13
4	Numerical Analysis	15
4.1	Parameters of the simulated system	15
4.2	The impact of the measurement time	17
4.3	The impact of the detection efficiency	17
4.4	The impact of the electronic noise	18
4.5	The impact of parasitic pulses	19
4.6	The impact of the sample emission intensity	20
5	Experimental demonstration	23
5.1	The measurement set-up	23
5.2	Configurations of the set-up	25
5.3	The data acquisition system	28
5.4	The characteristics of the recorded continuous signals	30
5.5	The estimation of calibration factors	32
5.5.1	The gate factors	33
5.5.2	The integral of a neutron induced pulse	33
5.6	Estimation of the detection rates	34
5.6.1	Singles rates	35
5.6.2	Doubles rates	36
6	Conclusions	38

Chapter 1

Introduction

The most common method for the passive assay of special nuclear materials is the so-called multiplicity counting technique [4, 5]. It is based on the counting of neutron induced pulses in single, double and triple coincidence in thermal neutron counters. The rate of detecting single counts and double and triple coincidences, called the singles, doubles and triples rates, serves three independently measured quantities, from which three parameters on an unknown item can be determined. The basis of the unfolding of the unknown parameters is that one can derive theoretical formulae for the multiplicity rates as functions of the unknown parameters of the sample in closed analytical form. Since these formulae, based on expressions of the factorial moments of the number of neutrons emitted from the item in one source event (spontaneous fission or (α, n) reaction) which are converted to multiplicity rates, are in analytical form, they can be inverted to determine the unknown parameters, primarily the fission rate of the spontaneously fissioning material (and hence its mass).

Pulse counting techniques are a well-established and effective method, but they also have some disadvantages. The dominating drawback is the existence of the dead time in the pulse counting, which leads to the loss of counts. Although there exist methods to remedy this problem both in the detection chain, as well as methods for correcting in the theory for the effects of the dead time, even these improvement and correction methods have their limitation, hence the problem still does exist. For instance dead time corrections become inapplicable for very high count rates, where the majority of the counts are lost. Such is the case of measurements in a spent fuel pool.

Another problem, although it is only technical and not methodological, is the recent shortage of ^3He . This in turn leads to a short supply of He-3 detectors, which are the prime instrument of multiplicity counting with thermal neutrons.

The above circumstances led us a few years ago to seek for an alternative way of performing multiplicity analysis, which offers a remedy for the above problems. We suggested to use the continuous signals of ionisation chambers, notably fission chambers, to extract the same statistical information about the item as the pulse counting method does. To this end it was necessary to develop a stochastic theory of fission chamber signals for detecting neutrons generated with a compound Poisson distribution, which is the case of the random number of neutrons emitted from an item with the emission events following an exponential time distribution. For the starting point we had already available a stochastic theory of fission chamber signals, due to detection of neutrons, arising from a pure Poisson distribution [6], used originally for the development of the theory of higher order Campbelling methods. This theory was first extended for detecting neutrons simultaneously from a compound Poisson distribution [1], and then to the case when account was taken to the fact the group of neutrons leaving the item simultaneously, will not be detected simultaneously, rather each neutron will be detected with an individual random time delay.

In two steps, first the consequences of this fact were explored [2], then a method was suggested to unfold the multiplicity rates from the integral of the covariance and bi-covariance of the signals of two and three detectors, respectively [3].

Although the validity of the formulae was verified by some simple Monte-Carlo simulations, the performance of the method under real measurement conditions is not obvious, where the effect of the finite measurement time, the presence of parasitic noise, and the difference in the detector efficiencies might affect the performance of the method and even its applicability in practical cases. Hence, and extensive numerical and experimental work was performed to clarify these questions. On the one hand, a system of Monte-Carlo codes were written to simulate a realistic experimental scenario, to simulate time-resolved detector signals. These simulated signals were then evaluated by the same tools as the measured signals. On the other hand, a dedicated experiment was designed and performed at the Institute for Integrated Radiation and Nuclear Science (KURNS), Kyoto University, by using a spontaneously fissioning neutron source (^{252}Cf) and four fission chambers. Measurements were made with and without surrounding the source with fissile material. The experiments were performed at a low count rate, such that the measurements would be evaluated by pulse counting (with software methods) and by the new method of analysing the continuous detector signals. This way the equivalence of the pulse counting and the new method could be verified.

Because of some limitations in the experiment, i.e. low detector efficiency, only the singles and the doubles rates could be determined. These verified the equivalence and hence the feasibility of the new method to determine the singles and doubles rates. Due to the (intentionally chosen) low count rate, the advantage of the new method what regards its insensitivity to the dead time effect, could not be demonstrated experimentally. This was demonstrated by the numerical simulations. The simulation software, on its turn, was validated by the good agreement it showed with the measurements at low count rates.

The structure of the rest of the report is as follows. Chapter 2 summarises the principles of multiplicity counting both with the traditional pulse counting and with the analysis of continuous signals. Chapter 3 describes the simulations software and its functions. Chapter 4 presents the numerical analysis performed and discusses the results. Chapter 5 describes the experimental setup, the measurements made, and a discussion of the results. The report is closed with a summary and conclusions.

Chapter 2

Theory of multiplicity counting

The objective of neutron multiplicity counting is the determination of the fissile mass of spontaneously fissioning materials, mostly plutonium. Figure 2.1 shows the conceptual scheme of the measurement. The measured sample is located inside a cavity which is open to air at atmospheric pressure. The cavity is surrounded by a large number (usually several dozens) of neutron detectors, most often ^3He -filled proportional counters, which measure neutrons emitted spontaneously from the sample. The space between the detectors is filled with polyethylene to thermalize the fast fission neutrons.

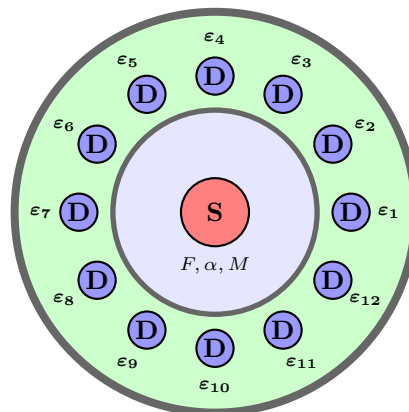


Figure 2.1: A conceptual view of the experimental setup of a multiplicity counting measurement, in which a heavy-nuclide sample (S), emitting neutrons spontaneously, is surrounded by a large number of neutron detectors (D).

The procedure of estimating the sample mass requires the mathematical formulation of the detector response. Both in the case of the traditional pulse counting as well as in the case of analysing continuous detector signals, this is based on Böhnel’s concept of superfission [7], a stochastic model of the neutron emission process in the sample. In the following, the superfission concept is summarized first briefly using the notations of [8]. Then, the procedure of extracting the sample mass is described in the pulse counting approach as well as with continuous signal analysis.

2.1 The emission of neutrons – the superfission concept

Neutrons within the sample are initially generated in two processes spontaneously. The primary source of neutrons is spontaneous fission. The total intensity of spontaneous fission in the sample

is $Q_f \equiv F$ and the probability mass function of the number of emitted neutrons is $p_{sf}(n)$ whose k th order factorial moments are denoted by $\nu_{sf,k}$. In addition, single neutrons are produced in (α, n) reactions induced by alpha-particles originating from the alpha-decay of plutonium isotopes with an intensity Q_α . In order to quantify the number of these reactions in the sample, it is customary to introduce the alpha-ratio defined as

$$\alpha = \frac{Q_\alpha}{Q_f \nu_{sf,1}}, \quad (2.1)$$

which is the ratio of the average number of neutrons produced in (α, n) reactions and spontaneous fission per unit time (unknown in a measurement). From a mathematical point of view, it is beneficial to combine spontaneous fission and (α, n) reaction into a single source event, which occurs at a rate

$$Q_s = Q_f + Q_\alpha = Q_f(1 + \alpha \nu_{sf,1}) \quad (2.2)$$

and at which neutrons are emitted according to the probability mass function

$$p_s(n) = \frac{Q_\alpha}{Q_s} \delta_{1,n} + \frac{Q_f}{Q_s} p_{sf}(n). \quad (2.3)$$

Each neutron emitted in a source event then either causes an induced fission with probability p , releasing neutrons with a probability mass function $p_i(n)$ whose factorial moments of order k are denoted as $\nu_{i,k}$, or they escape the sample with a probability $1 - p$ (neutron capture is negligible). The same is valid for every neutron born in induced fission as well. This multiplication effect of the sample is quantified by the net leakage multiplication factor defined as

$$M = \frac{1 - p}{1 - p \nu_{i,1}}, \quad (2.4)$$

which gives the expected number of neutrons that leave the sample as a result of a *single emitted source neutron*.

The term ‘‘superfission’’ refers to the fact that the internal multiplication in the item, between the source emission and the emission of the neutrons from the sample, is assumed to be instantaneous. The internal multiplication means that the number distribution $P(n)$ of the neutrons leaking out from the item will be shifted to higher neutron numbers, as compared to that of the original source event, hence the neutrons leaving the sample promptly in the time instant of the source emission can be interpreted as the result of a ‘‘superfission’’ event. Due to the instantaneous development of the fission chains in the item, the superfission events have the same intensity as the original source emission events Q_s (given in Equation (2.2)). The distribution $P(n)$ can be calculated from simple master equations [7, 5]. For the purposes of multiplicity counting, one usually uses the first three factorial moments ν_1 , ν_2 and ν_3 (often referred to as the Böhnel moments) of this latter distribution [4]. In order to simplify the upcoming formulas, let us introduce the following modified form of these moments [8]:

$$\tilde{\nu}_k = \nu_k(1 + \alpha \nu_{sf,1}). \quad (2.5)$$

The first three of the modified Böhnel moments can be written as [8]

$$\tilde{\nu}_1 = M \nu_{sf,1} (1 + \alpha), \quad (2.6a)$$

$$\tilde{\nu}_2 = M^2 \left[\nu_{sf,2} + \left(\frac{M - 1}{\nu_{i,1} - 1} \right) \nu_{sf,1} (1 + \alpha) \nu_{i,2} \right], \quad (2.6b)$$

$$\begin{aligned} \tilde{\nu}_3 = M^3 \left[\nu_{sf,3} + \left(\frac{M - 1}{\nu_{i,1} - 1} \right) [3 \nu_{sf,2} \nu_{i,2} + \nu_{sf,1} (1 + \alpha) \nu_{i,3}] \right. \\ \left. + 3 \left(\frac{M - 1}{\nu_{i,1} - 1} \right)^2 \nu_{sf,1} (1 + \alpha) \nu_{i,2}^2 \right]. \end{aligned} \quad (2.6c)$$

2.2 Traditional multiplicity counting

In the traditional form of a multiplicity counting measurement the information on the sample is extracted from the counting statistics of the neutron detectors (most frequently ^3He -gas-filled detectors) which are operated in the pulse counting mode. Specifically, the detection rates of the first three k -tuplets (k detected neutrons originating from the same sample emission) are determined [8]; these are called the *singles*, *doubles* and *triples* rates.

Let us assume that the measurement is performed using N detectors. Let ε_i denote the detection efficiency of the i th detector, i.e., the probability, that an emitted neutron is detected by the i th detector. Then

$$\varepsilon = \sum_{i=1}^N \varepsilon_i \quad (2.7)$$

is the efficiency of the entire detection system, i.e., the probability, that an emitted neutron is detected by one of all the detectors. The *singles*, *doubles* and *triples* rates can then be written as [8]:

$$S = F \tilde{\nu}_1 \varepsilon \quad (2.8a)$$

$$D = F \frac{\tilde{\nu}_2 \varepsilon^2}{2} f_d \quad (2.8b)$$

$$T = F \frac{\tilde{\nu}_3 \varepsilon^3}{6} f_t, \quad (2.8c)$$

Here F is the spontaneous fission intensity defined in Section 2.1, $\tilde{\nu}_i$ are the modified Böhnel moments defined by (2.6). The quantities f_d and f_t are called the doubles and triples “gate factors” and were introduced empirically to the formulae. They account for the loss of counts caused by the combination of the finite counting window as well as the random migration time of neutrons in the moderator which makes neutrons from the same sample emission arrive non-simultaneously to the detectors.

By inserting expressions (2.6) of the Böhnel moments into expressions (2.8) of the detection rates, a system of non-linear algebraic equations is obtained which can be solved analytically for the three sample parameters, F , α and M in terms of S , D and T [8]. The sample mass can then be deduced from the obtained value of F [4].

2.3 Multiplicity counting from continuous signals

In the new form of multiplicity counting, the fluctuating voltage signals of neutron detectors (primarily fission chambers) are analysed directly in order to obtain information on the sample. In particular, certain well-chosen moments up to the order of three (or integrals of these moments) are determined from which the same information on the sample can be obtained as from the singles, doubles and triples rates.

The derivation of the expressions of the moments is based on a stochastic model of the continuous signals of neutron detectors introduced in Reference [6]. The model assumes that every detected neutron generates a voltage pulse with a deterministic (constant) shape $f(t)$ and with a random amplitude \mathbf{a} characterized by a probability density function $w(a)$. The migration time of the neutrons in the moderator is represented by a random time delay τ , having a probability density function $u(\tau)$, between their emission and subsequent detection.

Using this model, several moments of the signals have been calculated. In References [1] and [2], expressions were derived for the one-point (in time) moments including the mean, variance and covariance of the signals. It was shown that when the average value of the time delay τ is much

larger than the typical width of the pulse (which is always the case in thermal detection systems) every moment, with one exception, vanishes due to the temporal separation of detections induced by neutrons from the same sample emission. The only non-vanishing moment is the mean value of the signal, which is invariant to the delay and, considering the signal of the i th detector, takes the form:

$$\kappa_i = F \tilde{\nu}_1 \varepsilon_i \langle a \rangle_i I_i. \quad (2.9)$$

Here F and $\tilde{\nu}_1$ are the same as before; $\langle a \rangle_i = \int_0^\infty a w(a) da$ is the mean pulse amplitude in detector i , whereas

$$I_i = \int_0^\infty f(t) dt \quad (2.10)$$

is the integral of the shape of the pulses in detector i . As a consequence of the above, in thermal systems only the first Böhnel moment $\tilde{\nu}_1$ (related to the singles rate in traditional multiplicity counting) can be recovered from the signals using the mean value.

In order to remedy this shortcoming, in Reference [3] the set of calculated moments was extended to the two- and three-point moments (in time), including the covariance function and bicovariance function of the signals. It was found that the integrals of these moments do not vanish even for large values of the random delay time τ of the detection. Two of them, namely the integrals of the covariance function of two signals as well as the bicovariance function of three signals, are especially favourable as they are completely independent of the delay. Considering three distinct detectors i , j and k , they take the form

$$\text{Cov}_{i,j} = F \frac{\tilde{\nu}_2}{2} \varepsilon_i \varepsilon_j \langle a \rangle_i \langle a \rangle_j I_i I_j \quad (2.11)$$

and

$$\text{Cov}_{i,j,k} = F \frac{\tilde{\nu}_3}{6} \varepsilon_i \varepsilon_j \varepsilon_k \langle a \rangle_i \langle a \rangle_j \langle a \rangle_k I_i I_j I_k, \quad (2.12)$$

respectively. Using these two quantities, the second and third Böhnel moments $\tilde{\nu}_2$ and $\tilde{\nu}_3$ can be recovered from the signals in thermal detection systems as well.

By inserting the Böhnel moments (2.6) into expressions (2.9)–(2.12), it would be possible to derive an analytical solution for the sample parameters F , α and M in terms of the quantities κ_i , $\text{Cov}_{i,j}$ and $\text{Cov}_{i,j,k}$. However, in order to make the two versions of multiplicity counting readily comparable, it is more appropriate to express the traditional S , D and T rates with the quantities derived from the moments of the signals. In particular, by first inserting (2.7) into (2.8) then utilizing (2.9)–(2.12), one can show that the following expressions hold:

$$S = \sum_{i=1}^N \frac{\kappa_i}{\langle a \rangle_i I_i}, \quad (2.13)$$

$$D = \sum_{i=1}^N \frac{\kappa_i}{\langle a \rangle_i^2 I_i^2} \left(\frac{1}{N-1} \sum_{\substack{j=1 \\ j \neq i}}^N \frac{\text{Cov}_{i,j}}{\kappa_j} \right) + 2 \sum_{i=1}^N \sum_{j=i+1}^N \frac{\text{Cov}_{i,j}}{\langle a \rangle_i \langle a \rangle_j I_i I_j} \quad (2.14)$$

and

$$\begin{aligned}
 T = & \sum_{i=1}^N \frac{\kappa_i^2}{\langle a \rangle_i^3 I_i^3} \left(\frac{1}{(N-1)(N-2)} \sum_{\substack{j=1 \\ j \neq k \neq i}}^N \sum_{k=1}^N \frac{\text{Cov}_{i,j,k}}{\kappa_j \kappa_k} \right) \\
 & + 3 \sum_{i=1}^N \sum_{j=1, j \neq i}^N \frac{\kappa_i}{\langle a \rangle_i^2 I_i^2 \langle a \rangle_j I_j} \left(\frac{1}{N-2} \sum_{\substack{k=1 \\ k \neq i \neq j}}^N \frac{\text{Cov}_{i,j,k}}{\kappa_k} \right) \\
 & + 6 \sum_{i=1}^N \sum_{j=i+1}^N \sum_{k=j+1}^N \frac{\text{Cov}_{i,j,k}}{\langle a \rangle_i \langle a \rangle_j \langle a \rangle_k I_i I_j I_k}.
 \end{aligned} \tag{2.15}$$

Chapter 3

Computational tools for simulating and analysing continuous signals

An application named `multiplicity counting measurement simulator` (in the continuation referred to as `MCM simulator`) was created that can produce continuous detector signals similar to those obtained in a real multiplicity counting measurement. To ensure a good performance, the program has been implemented in the C++ language. This program, described in detail in Section 3.2, is used for the numerical study presented in Section 4. Another C++ application called `continuous signal analyzer` (in the following: `CS analyzer`) was also created for the (off-line) analysis of the continuous detector signals generated by the `MCM simulator`. The purpose of the program is to provide estimates for the mean value as well as for the integrals of the covariance and bicovariance functions of sampled continuous signals. A description of the algorithms behind this program is given in Section 3.3. Signals submitted to `CS analyzer` for analysis are expected to be in a well defined file format, which is described in Section 3.1. Since both the simulation tool `MCM simulator` as well as the A/D converter used in the experiments (see Section 5.3) was programmed to produce signals in this format, the program `CS analyzer` was used to analyse both simulated measurements in Section 4 as well as real ones in Section 5.

3.1 The digital representation of signals

In order to make the voltage signal produced by a neutron detector suitable for digital analysis, it must be sampled with some time resolution Δt . From a data representation point of view, this results in a data sequence y_1, y_2, \dots , where y_i represents the observed voltage at time $i \cdot \Delta t$. Stored on a computer, such a sequence might take up a large amount of space. For example, when the amplitude values are represented as 32 bit numbers, then a 60s long signal sampled at 10 ns time resolution makes up 22.4 Gb of data. In order to minimize the required storage capacity, a special recording technique and an associated data format has been designed and will be described in the following.

The process of recording a signal is illustrated in Figure 3.1. When the observed count rate is high and consecutive pulses overlap, every recorded sample must be stored individually. On the other hand, when the count rate is low, pulses might be far from each other, separated by fluctuating background noise. Since the fluctuating background is well represented by a single average value (characteristic to the entire signal), these sections can be stored in a compressed format by recording only their sizes. A simple algorithm has been created to select between uncompressed and compressed recording modes. The algorithm has four parameters: a threshold voltage $V_{\text{threshold}}$, the head size N_{head} , the tail size N_{tail} and the idle size N_{idle} . Whenever the signal goes above $V_{\text{threshold}}$ and remains there for at least N_{idle} samples, individual values are

getting stored starting from N_{head} samples before the crossing point. Compression begins after N_{tail} consecutive samples were below $V_{\text{threshold}}$. The optimal value for $V_{\text{threshold}}$ is to be slightly above the background noise; the values of N_{head} and N_{tail} must be chosen based on the shape of the pulses; for N_{idle} a value between 1 and 3 is sufficient.

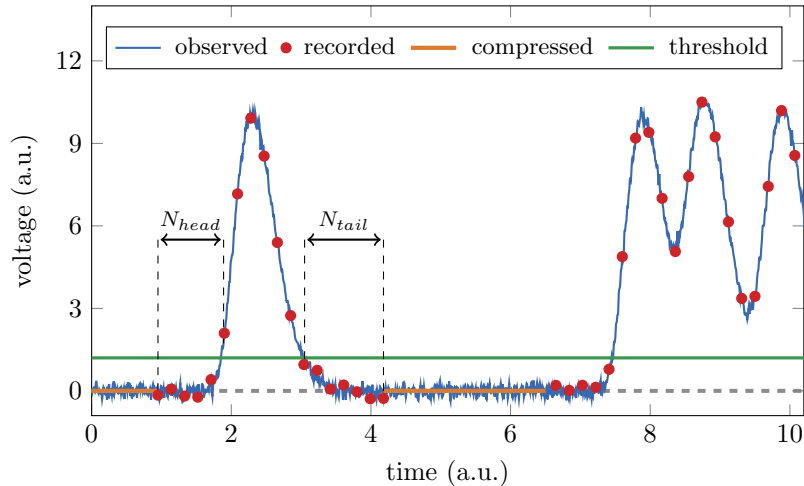


Figure 3.1: Illustration of the digitization process of continuous detector signals.

This same algorithm has been implemented by the application, presented in Section 4, that produces simulated signals as well as by the data acquisition device, described in Section 5.3, that records measured signals. Both tools store signals in files with the `time resolved signal format`. The structure of this file format is shown in Figure 3.2. It begins with a header block that contains four items: `resolution` contains the time resolution used to sample the signal; `size` contains the number of samples recorded (including samples in compressed sections); `baseline` contains an average background value observed between detections; `compression token` contains a value which is outside the range of the possible amplitude values and which indicates the beginning of a compression block. The header block is then followed by an arbitrary number of blocks, each of which is either a `data block` or a `compression block`. The `data block` represents an uncompressed signal section and might contain an arbitrary number of `signal amplitude` items, each holding a sampled amplitude value. The `compression block` represents a compressed signal section and has two items: `compression token` indicates the start of the block and `section size` holds the size of the compressed section. Upon analysis, the amplitude of the compressed sections is assumed to have the value of `baseline`.

3.2 The simulation of signals

The simulation of the output of a multiplicity counting measurement is a two step process performed by a pair of programs that together form the tool `MCM simulator` introduced earlier. Because the simulation involves large amounts of I/O operations, both programs were implemented in the C++ language to ensure good performance. The complete simulation process is illustrated in Figure 3.3 and is described in the following.

In the first step, the times of detections are determined by the program `detection time simulator`. The user can define a neutron emitting sample and a detector array containing an arbitrary number of detectors. The emission intensity and the multiplicity distribution of the sample can be specified. Each detector is associated with its own detection efficiency and time delay distribution. The distribution of the time delay can either be selected from a predefined set

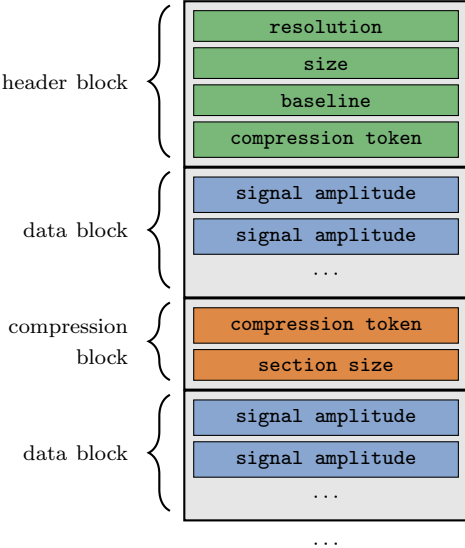


Figure 3.2: The structure of a file with the time resolved signal format.

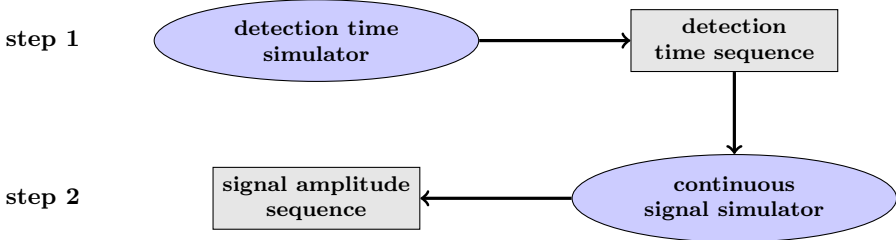


Figure 3.3: The two step process of simulating continuous signals.

(including the gamma, exponential, uniform or constant distributions), or its probability density function can be provided in a tabulated form. Using these parameters, the program calculates a sequence of detection times and writes them into a separate file for each detector.

In the second step, the continuous detector signals, sampled with some time resolution, are determined from the times of detections by the program `continuous signal simulator`. Since the program is only able to create one signal at a time, it must be run for each detector separately in order to produce the complete output of the simulated measurement. Input to the program is a file, obtained in the first step, containing the sequence of detections in the particular detector. The user can then specify the time resolution of the output signal, as well as the shape and amplitude distribution of the pulses generated by the individual detections. The shape of the pulses can either be selected from a predefined set (including the rectangular, exponential or double exponential shapes) or can be provided in a tabulated form. In a similar way, the amplitude distribution can also be selected from a predefined set (exponential, gamma, log-normal or constant distribution) or it can be given in a tabulated form. At each detection, a pulse is generated and the cumulative value of all the pulses is calculated for each discrete time instant. The signal values are then written into a file in the `time resolved signal format`, described in Section 3.1.

3.3 The analysis of signals

Consider a set of signals, obtained either from simulation or from a measurement, being available in the `time resolved signal format`. The purpose of the application `CS analyzer` is to estimate the value and variance of a target quantity q , which can either be the mean value of one signal or the integrals of the covariance or the bicovariance functions of two or three signals, depending on the choice made by the user.

The general algorithm of providing an estimate for the value and variance of q is illustrated in Figure 3.4 and is explained in the following. The signals are divided into segments of equal size N ; given a time resolution Δt , the length of these segments in time is $T = N \cdot \Delta t$. For each segment, a value of the target quantity is calculated independently; let q_i denote the value obtained from segment i . The exact algorithm to calculate q_i in the case of the three target quantities will be specified below. Assuming that there are M segments in total, the unbiased estimator of the value of the target quantity is the sample mean

$$\mu_q = \frac{1}{M} \sum_{i=1}^M q_i. \tag{3.1}$$

The standard deviation of this estimator is

$$\sigma_q = \sqrt{\frac{s_q^2}{M}}, \tag{3.2}$$

where s_q^2 denotes the unbiased estimator of the sample variance, which is given by

$$s_q^2 = \frac{1}{M-1} \sum_{i=1}^M (q_i - \mu_q)^2 = \frac{1}{M(M-1)} \left[M \sum_{i=1}^M q_i^2 - \left(\sum_{i=1}^M q_i \right)^2 \right]. \tag{3.3}$$

We shall now specify the mathematical form of q_i in the case of the above mentioned three analysis types. Within the i th segment, let $y_{k,1}, y_{k,2}, \dots, y_{k,n}$ denote the samples of the signal of

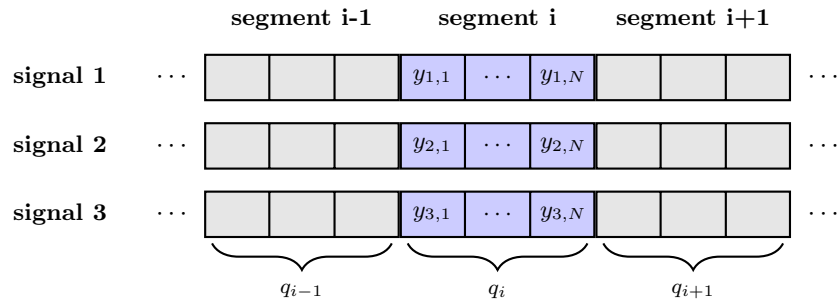


Figure 3.4: An illustration of how the signals are divided into segments during analysis.

detector k ($k = 1, 2, 3$). Let us further define the quantity

$$I_k(x) = \Delta t \sum_{j=1}^N (y_{k,j} - x), \quad (3.4)$$

which is a numerical approximation of the integral of the selected segment of signal k after it has been shifted by a constant value x . Then for the mean value of one signal (say that of 1) we can write

$$q_i = \frac{I_1(0)}{T} = \frac{1}{N} \sum_{j=1}^N y_{1,j}. \quad (3.5)$$

For the integral of the covariance function of two signals (say that of 1 and 2) we get:

$$q_i = \frac{I_1(\mu_{\kappa,1}) I_2(\mu_{\kappa,2})}{T} = \frac{\Delta t}{N} \left(\sum_{i=1}^N y_{1,i} - \mu_{\kappa,1} \right) \left(\sum_{i=1}^N y_{2,i} - \mu_{\kappa,2} \right), \quad (3.6)$$

where $\mu_{\kappa,1}$ and $\mu_{\kappa,2}$ denote the estimate of the mean value of signals 1 and 2. Similarly, when estimating the integral of the bicovariance functions of signals 1, 2 and 3, then q_i takes the form:

$$\begin{aligned} q_i &= \frac{I_1(\mu_{\kappa,1}) I_2(\mu_{\kappa,2}) I_3(\mu_{\kappa,3})}{T} \\ &= \frac{\Delta t^2}{N} \left(\sum_{i=1}^N y_{1,i} - \mu_{\kappa,1} \right) \left(\sum_{i=1}^N y_{2,i} - \mu_{\kappa,2} \right) \left(\sum_{i=1}^N y_{3,i} - \mu_{\kappa,3} \right). \end{aligned} \quad (3.7)$$

Formula (3.5) follows directly from the definition of the mean value; formulas (3.6) and (3.7) can be obtained using the Wiener–Khinchin theorem [9].

Finally, let us discuss how the value of the segment size N should be selected in the analysis. In the case of estimating the integral of the covariance and bicovariance functions, the length of the segments (in time) should be longer than the temporal correlations that are present in the signals. This minimum length can be determined either directly by estimating the covariance and bicovariance functions, or indirectly by gradually increasing N in the analysis until the result does not change anymore. In the case of the mean value, although N does not affect the estimated value, the same choice as in the other two cases should suffice.

3.4 Verification of the simulation tools

To verify the correct behaviour of the simulation and analysis programs described in Sections 3.2 and 3.3 a measurement with three detectors was simulated and analyzed. The values

of the signal moments and the detection rates recovered from them were then compared with the theoretical predictions. The simulation considered a hypothetical sample with an emission intensity $10\,000\text{ s}^{-1}$ and an emission multiplicity $P(n) = 1/5$ (for $0 \leq n \leq 4$). The neutrons were detected with an exponentially distributed time delay having a mean value of $50\ \mu\text{s}$. Each detector had a 30% detection efficiency and, upon detection, produced a pulse with unit amplitude and an exponential shape $f(t) = e^{-t/\alpha}$, where $\alpha = 1\ \mu\text{s}$. A $100\,000\text{ s}$ long measurement was simulated and the signals were recorded with a time resolution of $\Delta t = 0.1\ \mu\text{s}$. During analysis, the signals were divided into segments of $T = 20\text{ ms}$.

Table 3.1 lists the estimated moments of the signals along with the reference theoretical values. One can see that there is an excellent agreement in the case of the mean value and the integral of the covariance function. Although the deviation is larger in the case of the integral of the bicovariance function, but the difference between the estimated and reference values is still between $1\ \sigma$. This result shows that the program **CS analyzer** is able to estimate the correct moments of the signals. The detection rates recovered from the estimated moments using formulas (2.13)–(2.15) and the reference theoretical values are shown in Table 3.2. The corresponding values in each case agree within $1\ \sigma$ uncertainty, which proves the correctness of the detection rate recovering formulas of Section 2.3.

Table 3.1: Estimated values of the mean, the integral of the covariance function and the integral of the bicovariance function from test signals and their comparison with reference values.

quantity	detector	value	
		reference	estimated
mean value (V)	A		$(5.9984 \pm 0.0098) \cdot 10^{-3}$
	B	$5.9994 \cdot 10^{-3}$	$(5.9993 \pm 0.0098) \cdot 10^{-3}$
	C		$(5.9993 \pm 0.0098) \cdot 10^{-3}$
integral of the covariance function (V^2s)	A–B		$(3.582 \pm 0.015) \cdot 10^{-9}$
	A–C	$3.599 \cdot 10^{-9}$	$(3.597 \pm 0.015) \cdot 10^{-9}$
	B–C		$(3.608 \pm 0.015) \cdot 10^{-9}$
integral of the bicovariance function (V^3s^2)	A–B–C	$1.62 \cdot 10^{-15}$	$(1.70 \pm 0.28) \cdot 10^{-15}$

Table 3.2: Estimated values of the singles, doubles and triples detection rates from test signals and their comparison with reference values.

quantity	value (s^{-1})	
	reference	estimated
singles rate	18000	17998.5 ± 1.7
doubles rate	16200	16183.4 ± 19.9
triples rate	7290	7652.3 ± 455.5

Chapter 4

Numerical Analysis

In References [1, 2, 3] some important characteristics of the newly proposed method of multiplicity counting have been revealed and discussed on a theoretical basis. There are, however, a number of factors that, although have a strong effect on the practical performance of the method, are difficult to investigate with an analytical approach. Among others, such factors might include: the duration of the measurement, the efficiency of neutron detection, the characteristics of the electronic noise superimposed on the detector signals, the characteristics of parasitic signal components (e.g. gamma pulses) or the characteristics of the neutron emitting sample.

The most efficient procedure to gain information on how these parameters affect the recovered values of the detection rates is by performing a computational study using simulated measurements, since it allows us to change systems parameters in a controllable way. Such an investigation involving the above mentioned five parameters is the topic of this section. The detector signals were simulated using the `MCM simulator` tool described in Section 3.2 and their moments were estimated with the `CS analyzer` program presented in Section 3.3. The singles, doubles and triples detection rates were then calculated using Equations (2.13)–(2.15) and the effect of the investigated parameters on their values are assessed.

4.1 Parameters of the simulated system

For the sake of simplicity, the neutron emission multiplicity of the simulated sample has been chosen to be the same as the spontaneous fission multiplicity of the ^{240}Pu . This multiplicity, which is given in Table 4.1, was used for every simulated measurement. In Section 4.6, the intensity of the emission events is varied in a wide range; in all other cases the value $Q = 10\,000\text{s}^{-1}$ is used. One must note that the sample described here is only hypothetical, since the multiplicity of a realistic sample would be a mix of the multiplicities of several even mass numbered Pu isotopes. Moreover, unlike it is assumed in Section 4.6, it could be affected by induced fission in the ^{240}Pu and (α, n) reactions in the sample. Nevertheless, this simplification does not affect the conclusions drawn from the results of the simulations.

Table 4.1: Multiplicity distribution of emitted neutrons (per emission event) of the simulated sample. The values are taken from Reference [10].

n	0	1	2	3	4	5	6
$P(n)$	0.066	0.232	0.329	0.251	0.102	0.018	0.002

The parameters of the detection system were chosen to represent a typical thermal multiplicity counter equipped with ^3He gas filled detectors [4, 10]. Although such a counter normally contains

dozens of neutron detectors, to simplify the simulation process, we have unified them into three “large” detectors which have identical parameters. As in the verification step in Section 3.4, the neutrons were assumed to arrive with an exponentially distributed time delay to the detectors. The mean delay was $\theta_{\text{delay}} = 50 \mu\text{s}$, which is typical in thermal systems, and was not varied in the simulations. The efficiency of the detectors was varied in Section 4.3; in every other case, the cumulative efficiency of all three detectors was 50% which gives an approximate efficiency of $\varepsilon = 16.66\%$ per detector.

Unlike in the verification, a realistic neutron induced pulse shape was considered here given by the function

$$f(t) = \frac{1}{c} \left(e^{-t/\theta_{\text{pulse},1}} - e^{-t/\theta_{\text{pulse},2}} \right) \quad \text{for } t \geq 0, \quad (4.1)$$

where the constant parameter c is chosen in a way that the amplitude of $f(t)$ is unity:

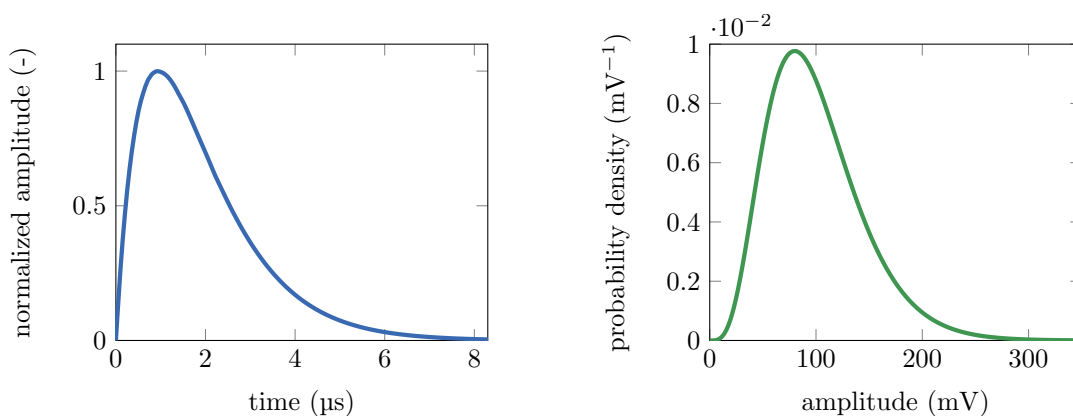
$$c = \left(\frac{\theta_{\text{pulse},2}}{\theta_{\text{pulse},1}} \right) \frac{\theta_{\text{pulse},2}}{\theta_{\text{pulse},1} - \theta_{\text{pulse},2}} - \left(\frac{\theta_{\text{pulse},2}}{\theta_{\text{pulse},1}} \right) \frac{\theta_{\text{pulse},1}}{\theta_{\text{pulse},1} - \theta_{\text{pulse},2}}. \quad (4.2)$$

The values chosen for the time constants are $\theta_{\text{pulse},1} = 1 \mu\text{s}$ and $\theta_{\text{pulse},2} = 0.9 \mu\text{s}$; this gives a characteristic pulse length of around $10 \mu\text{s}$ which is a typical value for thermal neutron detectors [10] and is close to the length of the pulses recorded in the measurements discussed in Section 5. A shape corresponding to these parameters is shown in Figure 4.1a and was used in each simulated measurement.

To model the size variation of consecutive pulses, their amplitude was assumed to follow the gamma distribution with probability density function

$$w(a) = \frac{1}{\Gamma(k) \theta_{\text{amplitude}}^k} a^{k-1} e^{-a/\theta_{\text{amplitude}}}, \quad (4.3)$$

where Γ denotes the gamma-function. The value $k = 5$ was selected for the shape parameter of the distribution and $\theta_{\text{amplitude}} = 20 \text{ mV}$ for the scale parameter; this gives a mean amplitude $\langle a \rangle = k \theta_{\text{amplitude}} = 100 \text{ mV}$ which is a realistic value for pre-amplified signals. The probability density function of the pulse amplitudes is shown in Figure 4.1b and, just as in the case of the shape, it was used without variation.



(a) The time evolution of the pulse shape.

(b) Probability density function of the pulse amplitude.

Figure 4.1: The characteristics of simulated pulses.

The signals generated with the above parameter values were recorded with a time resolution of $\Delta t = 0.05 \mu\text{s}$, which was chosen to be large enough to properly resolve individual pulses. To

assess its effect, an exceptionally long measurement was simulated in Section 4.2. In every other case, the duration of the simulated measurements was 1000 s which is a typical value in the case of multiplicity counting measurements [4]. During analysis, the signals were divided into 20 ms long segments.

4.2 The impact of the measurement time

According to Equation (3.2), the error of the estimated values of the moments of the detector signals is inversely proportional to the square root of the measurement time. To investigate how the measurement time affects the precision of the detection rates, a long measurement lasting 30 000 s, which is equivalent to about 8.3 hours, was simulated and analyzed. Figure 4.2 shows the change of the relative errors of the three detection rates with the measurement time.

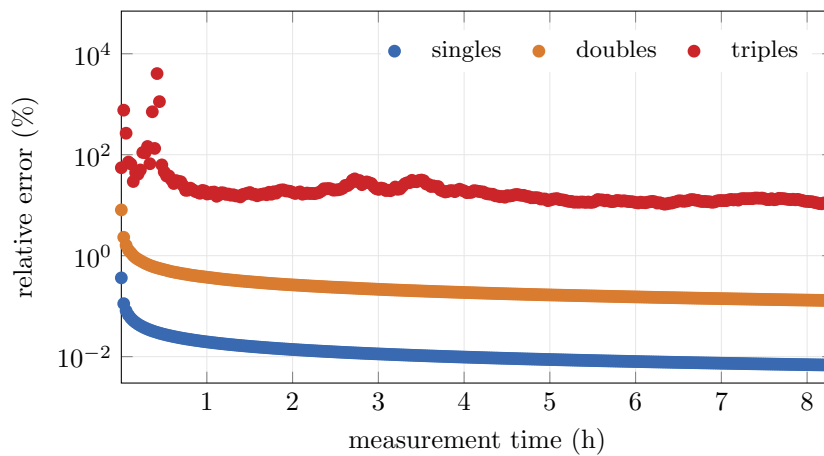


Figure 4.2: Relative errors of estimates of the singles, doubles and triples rates as a function of the measurement time.

As one would expect, the singles rate estimation provides the lowest relative error, while the triples rate estimation provides the largest. In the case of the singles rate, the relative uncertainty does not go above 1 % even for short measurement times; it reaches 0.1 % in a couple of minutes and 0.01 % in about 3 hours. The error of the doubles rate estimate reaches 1 % quickly and approaches 0.1 % after more than 8 hours. Compared with the singles and doubles rates, the estimate of the triples rate shows a much worse quality. On the time scale of minutes, relative errors as large as 1000 % can be observed; after 1 hour, the uncertainty approaches 10 % and does not decrease much by 8 hours. Moreover, unlike in the case of the other two detection rates, the relative uncertainty of the triples rates does not always decrease monotonically with the measurement time.

Because a large number of measurements had to be simulated in order to obtain the upcoming results, the duration of the simulated measurements was chosen to be 1000 s which is equivalent to around 16 minutes. Since the triples rates cannot reach convergence in such a short time (see Figure 4.2), in the following results are shown and conclusions are drawn only for the singles and doubles rates. The convergence issue of the triples rate will be dealt with in a future study.

4.3 The impact of the detection efficiency

Of all the parameters, the efficiency of neutron detection has most likely the largest influence on the recovery of the detection rates. As seen from Equation (2.8), the singles rate depends linearly

on the detection efficiency, while the doubles and triples rates are proportional to its second and third powers. For this reason, one of the primary goals when designing a multiplicity counting measurement is to achieve as high detection efficiency as possible. ^3He gas-filled detectors, which are used in the majority of cases in these types of measurements, can typically provide a 40%–60% efficiency for thermal neutrons; with thermal fission chambers applied in certain cases, on the other hand, the detection efficiency can be as low as 1% [4].

To illustrate its effect, the detection efficiency of the simulated system was varied in the range of 1%–80%. Figure 4.3 shows the values and the relative uncertainties of the estimated singles and doubles rates as a function of the efficiency. One can see that the estimated values of the detection rates show a good agreement with the theoretical expectations. The relative uncertainties of both the singles and doubles estimates show a fast decrease as the efficiency increases, although it is clearly faster for the doubles. These results confirm the preliminary suspicion that the neutron detection efficiency has a strong effect on the accuracy of the measurement.

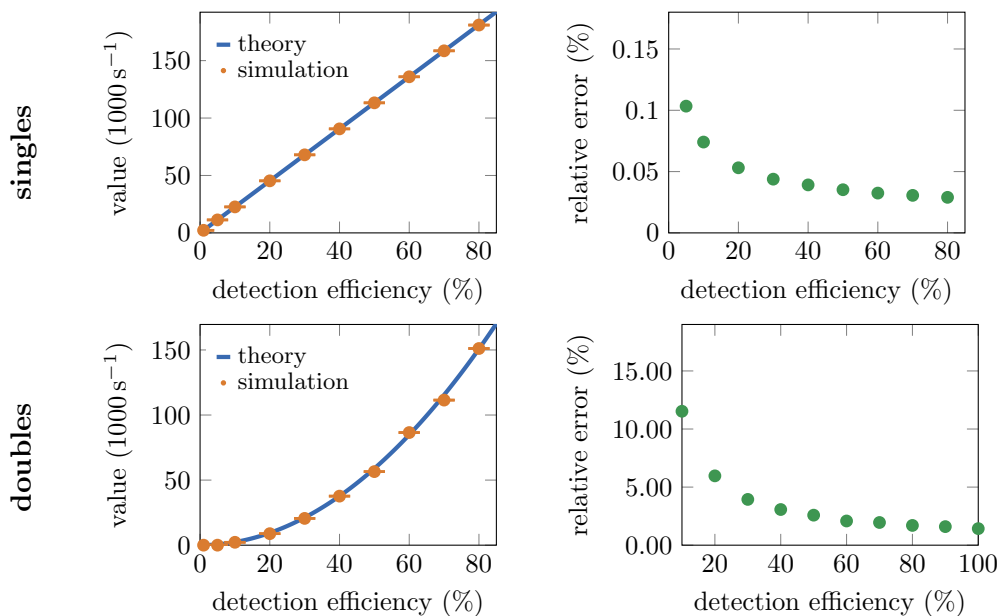


Figure 4.3: The value and uncertainty of the estimated singles and doubles rates obtained from simulated measurements as a function of the detection efficiency.

4.4 The impact of the electronic noise

The most significant sources of electronic noise in a radiation measurement are located at the beginning of the detection chain: the detector itself, as well as the pre-amplifier and its input stage. Since the noise generated in these elements undergoes the same amplification process as the primary signal, it can seriously degrade the information carried by pulses induced by detected particles. This is especially true for methods that rely on discrete pulse counting, since the noise can easily produce false counts in an integral discriminator [11]. On the other hand, higher-order Campbell techniques – which are also based on the central moments of continuous signals and hence can be considered as a close relative of the method presented in this paper – are known to be more resistant to the presence of noise [11].

To investigate whether the newly proposed method possesses such a resistance as well, electronic noise has been superimposed on the simulated neutron signals. Although it might not

always be the case in practice ¹, for simple analytical or numerical investigations it is often assumed that electronic noise is white and Gaussian (i.e. its power spectral density is constant in frequency whereas its amplitude distribution is normal with zero mean). For this reason, the same assumption was held in the present computational study. While keeping its mean value zero, the standard deviation of the noise varied in the range 0 mV–50 mV; the upper limit corresponds to half of the mean amplitude of neutron pulses.

The results are summarized in Figure 4.4. The blue horizontal lines on the two left graphs show the theoretically expected values of the singles and doubles rates in the case when there is no noise present. One can see that the recovered detection rates follow these lines closely, and the relative errors of the rates also seem to be independent of the noise amplitude. These results suggest that the procedure is rather insensitive to the presence of noise – at least of the white Gaussian type. In the case of the singles rate, this insensitivity comes from the fact that the noise – having a zero mean – does not contribute to the mean value of the recorded signal. In the case of the doubles rate, since the noise observed in two different signals is independent, their contribution to the covariance function will be zero.

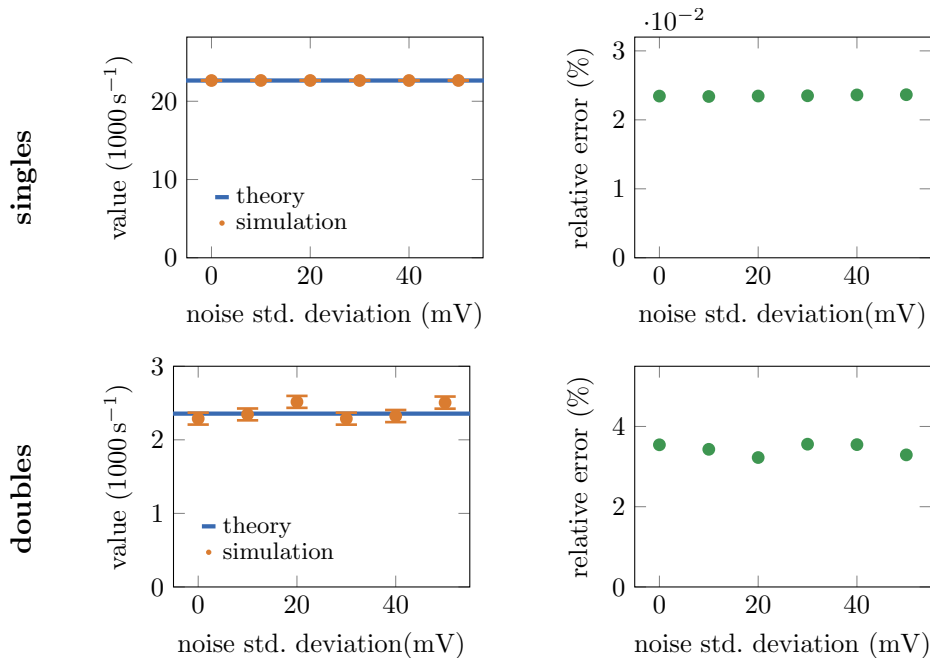


Figure 4.4: The value and uncertainty of the singles and doubles detection rates obtained from simulated measurements as a function of the standard deviation of the superimposed Gaussian white noise.

4.5 The impact of parasitic pulses

Every neutron detector will also be sensitive, to some degree, to particles of other radiation types as well. ³He-gas filled detectors, for example, are known to have a relatively high detection efficiency for gamma particles [11, 10]. Although less sensitive to gamma radiation, the α -decay of heavy isotopes in the fissile deposit of fission chambers might generate a considerable alpha

¹A recent study investigating the measured continuous signals of thermal fission chambers showed that the power spectral density of the noise is pink (inversely proportional to the frequency) and its amplitude distribution is close to normal [12].

background [11]. Most of the time, however, pulses induced by such parasitic detections have much smaller amplitudes than neutron induced pulses; in the case of alpha-induced pulses in fission chambers, the difference is typically a factor of 10 [11]. This fortunate property makes it possible to filter out the parasitic component of the detector signals. In pulse counting mode, small amplitude pulses can easily be differentiated against on an amplitude basis – at least at low count rates. At the same time, according to the higher-order Campbell theorem, the n th order central moment of the continuous signal is proportional to the integral of the n th power of the pulse, which provides these methods with an inherent capability of suppressing minority signal components [13].

To investigate how the presence of parasitic pulses affects the recovery of the singles and doubles rates, a secondary particle source is assumed in the simulations besides the neutron source. For the sake of simplicity, we shall assume that this secondary source is independent from the primary neutron source and its particles arrive in a homogeneous Poisson process with intensity $Q_{\text{parasitic}}$. This simple model describes well the α -particle induced signal of a fission chamber, or the gamma-signal produced by activation and/or fission products in the case of a ^3He detector. No attempt is made in the present study to simulate a correlated secondary source, such as prompt fission gamma radiation in the fissile sample, as this question will be addressed by future research activities. We shall further assume that parasitic pulses have the same shape as neutron pulses and a similar amplitude distribution, but their mean amplitude is smaller by a factor of 10. Because in practice the strength of the parasitic particle source depends heavily on the measurement conditions, the corresponding detection rate varied in the range $Q_{\text{parasitic}}=0\text{ s}^{-1}\text{--}15\,000\text{ s}^{-1}$ in the simulations; the upper boundary here is 1.5 times the intensity of neutron emissions.

Figure 4.5 shows the results. The blue horizontal lines on the two left graphs correspond to the true, theoretically calculated values of the singles and doubles rates. Two sets of simulated values are given for the singles rate. The first set, shown in orange, was obtained by completely disregarding the bias of the parasitic signal and applying Equation (2.13) directly to the mean values estimated from recorded signal. As one would expect, the singles rate obtained with this approach increases linearly with the parasitic detection rate and deviates from the true value. The second set of values, shown in green, which agrees with the theoretical expectations, was obtained by correcting for the bias of the parasitic pulses: the mean value of the parasitic signal component was subtracted from the mean value of the combined parasitic–neutron signal before using Equation (2.13) to obtain the singles rate. To apply this correction in practice, one could perform a background measurement with no neutron source present and register only the parasitic signal so that its mean value can be estimated. The doubles rate appears to be insensitive to the presence of the parasitic background. This is expected in the case of a Poissonian source, since its contribution to two different signals is statistically independent, hence their covariance function will be zero. Finally, one might observe that the relative errors of the singles and doubles estimates also have no dependence on the strength of the parasitic source.

4.6 The impact of the sample emission intensity

The primary factor that limits the applicability of traditional multiplicity counting is the dead time arising in the integral discriminator due to the overlapping of pulses. Since dead time losses can only be corrected for only to a certain extent, the method cannot be used to measure samples with high emission intensities such as spent nuclear fuel. On the other hand in Papers [1, 2, 3] we stated that one of the most appealing characteristic of the newly proposed version of multiplicity counting is the lack of dead time caused by pulse overlapping.

In order to illustrate the effect of dead time on the recovered detection rates, the sample emis-

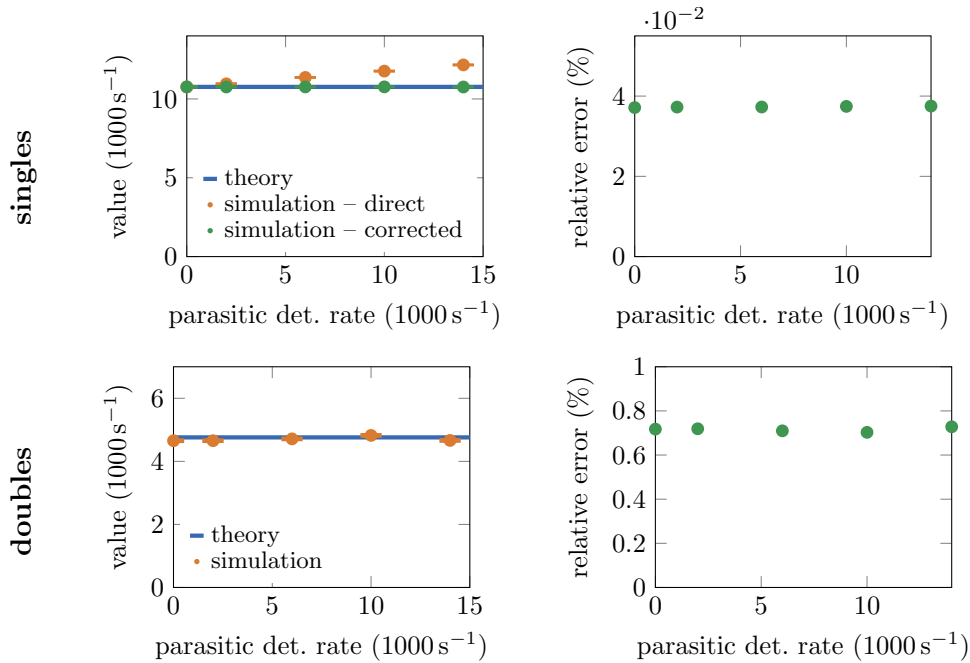


Figure 4.5: The value and uncertainty of the singles and doubles detection rates obtained from simulated measurements as a function of the parasitic particle detection intensity.

sion intensity was varied in the range of $Q_s=1000 \text{ s}^{-1}$ – $100\,000 \text{ s}^{-1}$. To compare the performance of the two versions of multiplicity counting, the singles and doubles rates have been determined both from the moments of the continuous signals as well as by pulse counting using a simple program that processes the recorded signals and counts pulses with a predefined threshold level. The detection rates obtained with pulse counting include the correction with the gate factors (see Equation (2.8)), but no dead time correction was applied.

The results are summarized in Figure 4.6. One can see that the singles and doubles rates obtained from the moments of the continuous signals show an excellent agreement with the theoretical expectations over the entire range of the emission intensity that was considered. At low emission rates, when pulses rarely overlap, the agreement is also good with the values obtained from pulse counting. However, as the emission rate increases, and the overlapping of pulses becomes more frequent, the detection rates underestimate the true values.

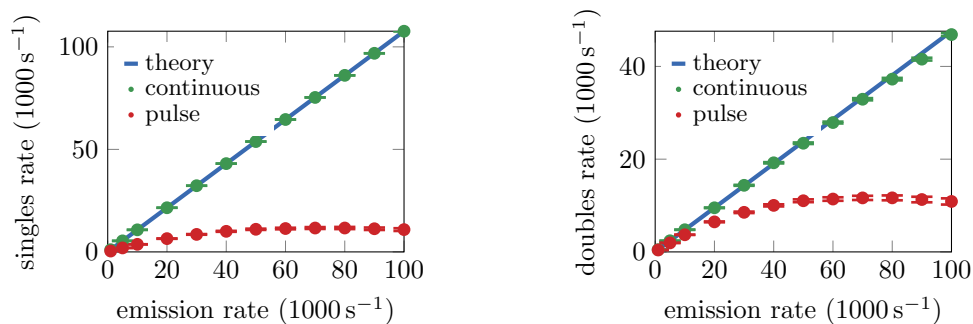


Figure 4.6: Singles and doubles detection rates obtained from simulated measurements as a function of the sample emission intensity.

At last it should be emphasized that the above results are only an illustration of a crucial

difference between the two versions of multiplicity counting and do not reflect their absolute performances. Specifically, the traditional approach is much more resistant to dead time in real applications for at least two reasons [4]. First, instead of 3, several dozens of neutron detectors are used whose signals are processed by 10–60 independent signal processing chains thus greatly reducing the frequency of pulse overlapping. Second, an integral discriminator responsible for the selection of pulses is a much more sophisticated tool [11] than the simple computer algorithm used in the simulations. Nevertheless, at large enough intensities the pulse counting approach will inevitably produce false results.

Chapter 5

Experimental demonstration

An experiment has been designed and performed in order to demonstrate the practical use of the new method of multiplicity counting by measuring a ^{252}Cf sample. The activity was carried out in a collaboration between the Budapest University of Technology and Economics, Chalmers University and the Kyoto University Institute for Integrated Radiation and Nuclear Science (KURNS) and took place at the Kyoto University Critical Assembly (KUCA) facility in Osaka, Japan. Our aim was to build a measurement set-up in which the detection rate is low enough not to cause overlapping pulses very often. This allowed us to measure the detection rates not only from the continuous signals, but – to serve as a reference – also with the pulse counting procedure.

Although the general purpose of multiplicity counting is to determine the fissile mass of a sample, no estimation of the mass was given in this measurement for two main reasons. First, in order to recover the mass from the detection rates, one needs to know the values of *a)* certain nuclear physical constants of the fissile isotopes, *b)* the detection efficiency and *c)* the gate fraction factors (at least for detection rates obtained with pulse counting) [4]. While the physical constants are generally known, the other two parameters are usually determined with a careful calibration of the multiplicity counter device [4]. In our measurement, we had no option to perform such a calibration. The second and more important reason is that the mass recovering procedure requires the knowledge of all three detection rates. However, as we shall see later, it was not possible to estimate the triples detection rate in our measurement set-up. For this reason, the primary goal of the measurement was to show that the newly proposed method is able to provide the same detection rates as traditional multiplicity counting.

5.1 The measurement set-up

KUCA is a multi-core facility consisting of two solid-moderated cores (A and B core) and a light-water moderated core (C core) [14]. The basis of the A core is a rectangular aluminum grid into which assemblies can be loaded. Each assembly consists of a rectangular aluminum frame into which plates of different materials (uranium, polyethylene, graphite, etc.) and thicknesses can be loaded horizontally (see Figure 5.4) similarly to how pellets are loaded into a fuel rod. This modular nature of the assemblies makes it possible to construct a large variety of measurement arrangements. The experimental set-up was assembled on the same grid that hosts core A, however, it was located outside the graphite reflector surrounding the core. The position of the set-up next to the core is shown in Figure 5.1.

In the following, the measurement set-up is described in detail. The description is best supported by images from the MCNP [15] model of the set-up shown in Figure 5.3, but actual photos of certain elements of the arrangement can also be seen in Figures 5.2 and 5.4. Since

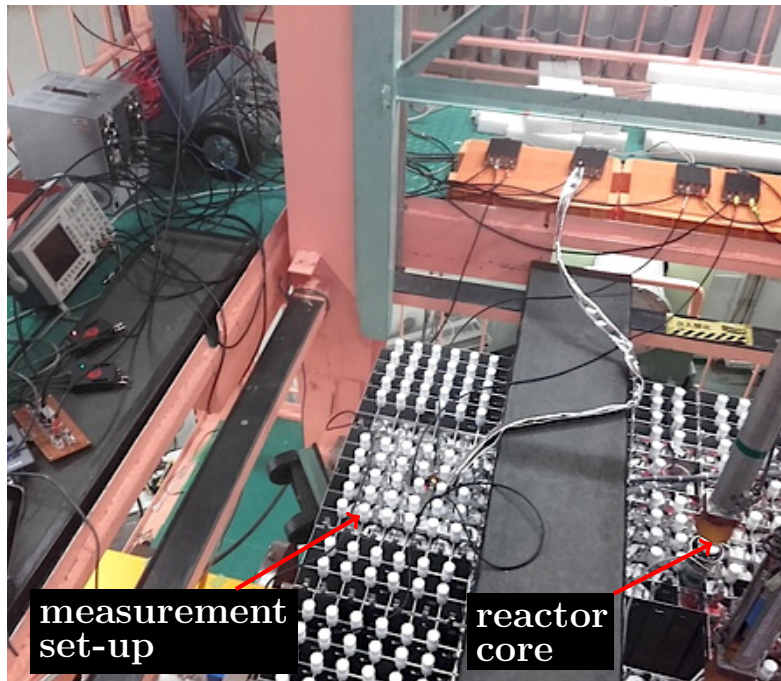


Figure 5.1: Photo showing the multiplicity counting measurement set-up next to the reactor core.

the facility was designed by the United States government, the sizes (and most other technical data) of its components are documented in imperial units [14]. Therefore, in the description that follows, the original documented values will be presented but approximate values in metric units will be presented as well.

As seen in Figure 5.3, the set-up consists of a 5×5 lattice of assemblies. Each assembly is loaded with rectangular cuboid plates with a $2 \text{ in} \times 2 \text{ in}$ ($50.8 \text{ mm} \times 50.8 \text{ mm}$) cross section and different thicknesses. Three different types of assemblies were built. We shall refer to these as *source assembly*, *detector assembly* and *moderator assembly*. Figure 5.4 shows actual pictures of these assemblies while being put together on site. In the following, the vertical structure of the assemblies and their positioning in the arrangement is described.

The central grid element in the arrangement is the source assembly which hosted three ^{252}Cf samples. Each sample was enclosed in a cylindrical aluminium casing with an approximate diameter of 2 mm and an approximate height of 10 mm. The registered activities (including α -decay and spontaneous fission) of the three samples on September 6, 2019 were 48.9 kBq, 48.9 kBq and 14.7 kBq, respectively. This gives a total activity of 112.5 kBq and a total neutron emission rate of 12930 s^{-1} . The samples were placed inside a $1/8 \text{ in}$ ($\approx 3.18 \text{ mm}$) thick polyethylene plate as shown in Figure 5.2. This plate was then placed in the middle horizontal plane of the source assembly (which was also the middle plane of the entire set-up).

Two versions of the source assembly were built in order to create two measurement configurations. In both versions, the central polyethylene plate (enclosing the californium samples) was surrounded by additional $1/8 \text{ in}$ ($\approx 1.18 \text{ mm}$) thick polyethylene plates from the top and the bottom. In one of the two versions, however, some of these polyethylene plates were replaced by 93.2% enriched uranium-aluminum alloy plates of equivalent thickness. Figures 5.3 and 5.4 show only this second version. A more detailed description of the two configurations and the motivation behind creating them will be given in Section 5.2.

The central source assembly was surrounded symmetrically by four detectors, each taking the

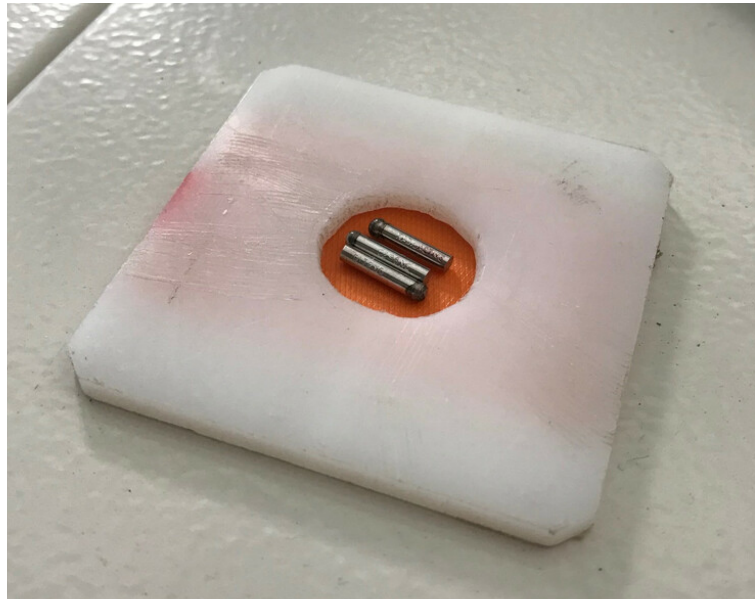


Figure 5.2: Three ^{252}Cf sources embedded into a polyethylene plate.

position of a fuel assembly. They are labeled with A–D on Figures 5.3 and 5.4 (and these same labels will be used to refer to the signals of the corresponding detectors as well). Each assembly was hosting one thermal fission chamber of the same type. A detailed technical description of the detectors (along with the entire data acquisition chain) will be given in Section 5.3. The detectors were positioned vertically in a way that their sensitive region lies symmetrically around the plane of the californium sources. From the top and the bottom, they were surrounded with polyethylene blocks of appropriate thicknesses.

All the remaining positions in the grid were occupied by moderator assemblies. The moderator assemblies were entirely filled with 1/8 in (≈ 3.18 mm) thick polyethylene plates. Two different densities of polyethylene were used, indicated by green (lower density) and yellow (higher density). The primary purpose of the polyethylene in the moderator assemblies as well as in the other two types of assemblies was to thermalize fast fission neutrons, thus increasing the probability of detection in the fission chambers and the induced fission in the uranium-aluminum plates (when present).

5.2 Configurations of the set-up

Since multiplication of the source neutrons in the fissile material of the item increases the leakage multiplications and hence the detection rate, two measurement configurations containing different amounts of fissile material were created in the hope that a significant difference between the detection rates obtained in them will be observed. The first configuration contained only the three samples of ^{252}Cf , located in the source assembly, and no surrounding fissile material; this configuration will be labeled as Cf in the subsequent sections. In the second configuration 90% enriched ^{235}U plates were placed inside the source assembly symmetrically above and below the californium to simulate a fissile item through the induced fission caused by the primary neutrons from the californium; it will be labeled as Cf+U.

The number of neutrons produced additionally in induced fission is sensitive to the amount and location of the uranium in the system: the uranium must be far enough from the californium so that neutrons thermalize by the time they reach it; on the other hand, if too much polyethylene

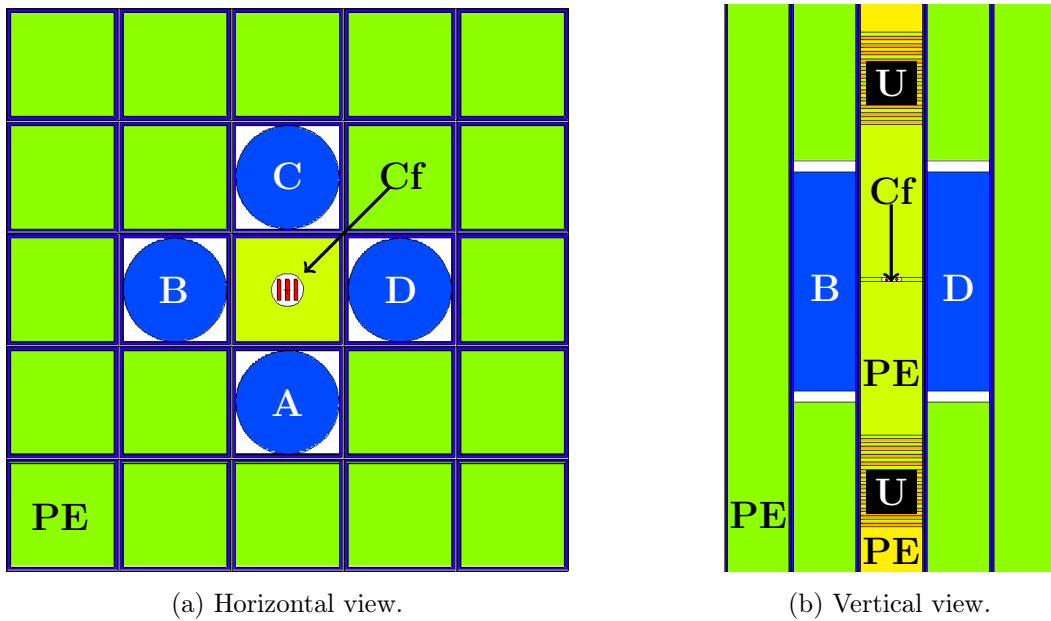


Figure 5.3: The MCNP model of the measurement set-up. The labels have the following meaning: Cf: ^{252}Cf source, U: U plate, PE: polyethylene (different colours correspond to different densities), A–D: detectors, white areas: air.

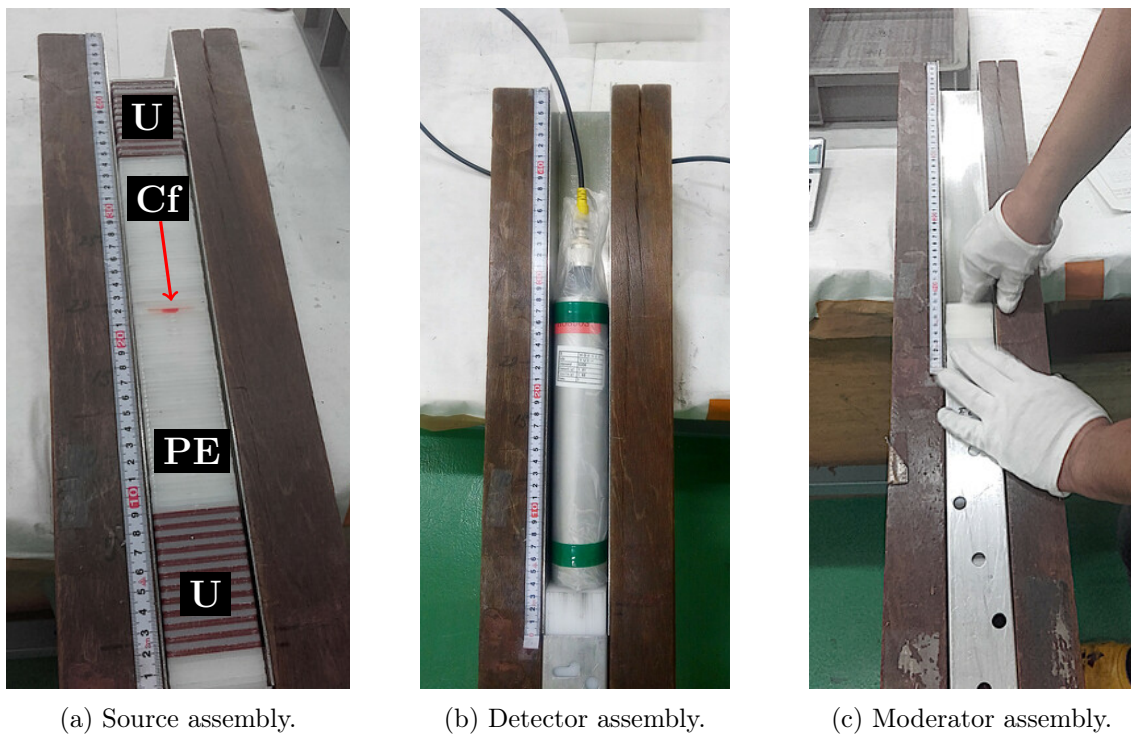


Figure 5.4: The three assemblies used in the measurement arrangement while being assembled.

is replaced by uranium, the neutrons do not get moderated. The final positioning of the uranium-aluminum plates in configuration Cf+U was determined by a simple numerical optimization using the MCNP model of the set-up. Models for seven variants of the central assembly were created that contained different amounts of uranium at different distances from the californium; these are labeled with B–H in Figure 5.5 (label A shows the variant with no uranium at all, used in configuration Cf). Simulations were performed to estimate the singles, doubles and triples detection rates by using each variant of the source assembly. The triples to singles ratio has been chosen as a measure of the effect of the uranium. Therefore the goal was to identify the configuration which produces the highest value for this ratio.

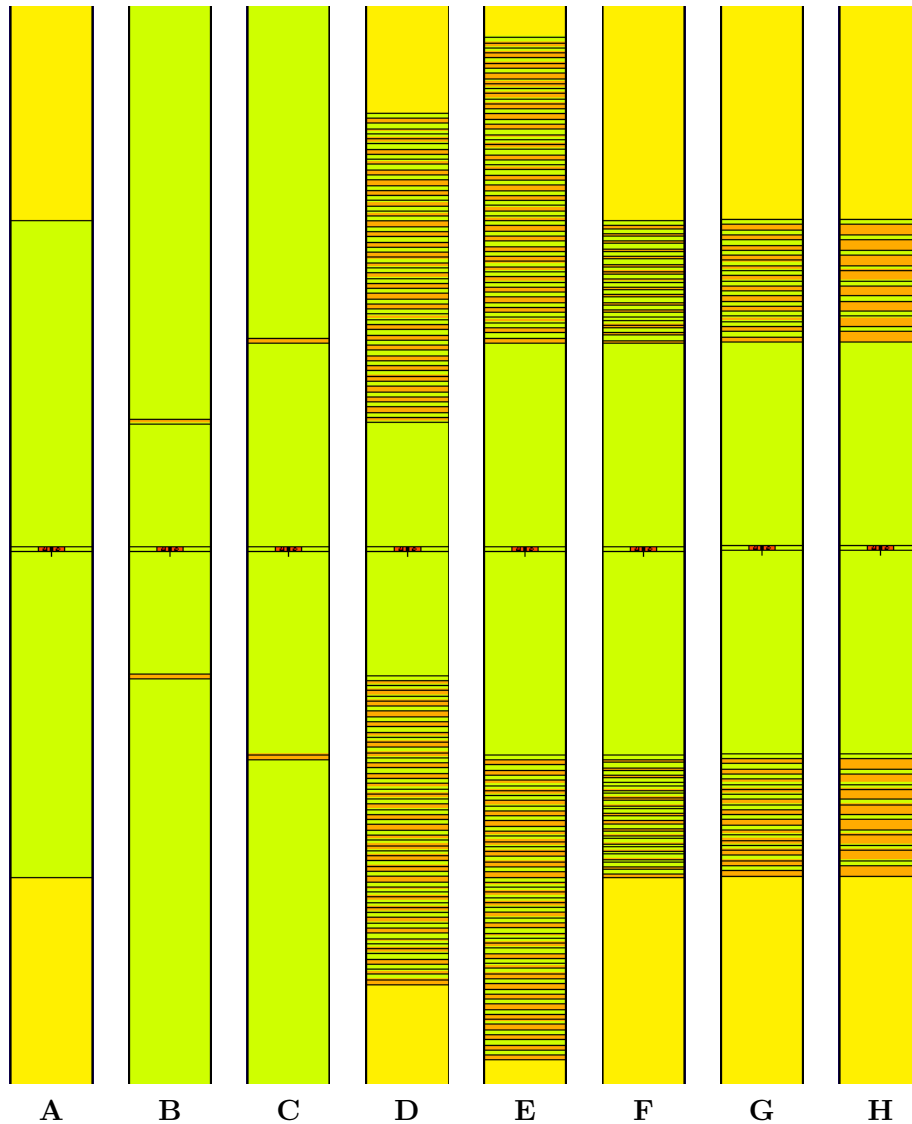


Figure 5.5: Variants of the central source assembly used for the optimization of the measurement arrangement. For the notations, see Fig. 5.3.

The results are listed in Table 5.1, where the labels of the variants that were built in the end are marked with bold. One can immediately see that there is no significant difference between the detection rates in configuration Cf (with variant A) and Cf+U (variants B–H). This suggests that the measurements will not be able to show any difference either. In any case, for realizing configuration Cf+U, variant G has been selected because it yields the highest triples to singles

ratio.

Another important thing to notice in Table 5.1 is the rather low value of the triples rates in both configurations. This is a consequence of the low detection efficiency of the system, which originates partly from the generally low internal efficiency of fission chambers (compared to other neutron detectors [11]) and partly from the low geometric efficiency due to the arrangement of the sample and the detectors. As a result, the triples rates are not expected to be measured with any good accuracy.

Table 5.1: Simulated values of the detection rates in the configuration shown in Figure 5.4.

configuration	detection rate (s^{-1})			triples to singles ratio (10^{-3})
	singles	doubles	triples	
A (Cf)	80.697 ± 0.283	3.984 ± 0.063	0.208 ± 0.014	2.58
B	79.773 ± 0.281	3.922 ± 0.062	0.202 ± 0.014	2.54
C	80.885 ± 0.283	4.029 ± 0.063	0.206 ± 0.014	2.55
D	79.092 ± 0.280	3.919 ± 0.062	0.203 ± 0.014	2.57
E	81.676 ± 0.284	4.130 ± 0.064	0.219 ± 0.015	2.68
F	81.513 ± 0.284	4.125 ± 0.064	0.215 ± 0.015	2.64
G (Cf+U)	81.585 ± 0.284	4.137 ± 0.064	0.220 ± 0.015	2.70
H	81.572 ± 0.284	4.147 ± 0.064	0.216 ± 0.015	2.65

Finally, while the values presented in Table 5.1 refer to the detection rates observed in all four detectors cumulatively, Table 5.2 shows the singles rates from one detector, the doubles rates from a pair of detectors as well as the triples rates from three detectors, in the two configurations Cf and Cf+U. These will be compared with the measured values in Section 5.6.

Table 5.2: Simulated values of the detection rates in configurations Cf and Cf+U.

quantity	value (s^{-1})	
	Cf	Cf+U
singles (per 1 detector)	20.174 ± 0.141	20.396 ± 0.142
doubles (per 2 detectors)	0.996 ± 0.031	1.034 ± 0.032
triples (per 3 detectors)	0.088 ± 0.009	0.093 ± 0.010

5.3 The data acquisition system

Figure 5.6 shows the layout of the detection, signal processing and data acquisition system used in the measurement. The output signal of every neutron detector is passed through a high-frequency pre-amplifier. The amplified voltage signal then continued on two paths. On the one hand, it was sent to a high-resolution A/D converter to produce a sampled (digitized) continuous signal. On the other hand, it was submitted to a chain containing an amplifier, a discriminator and a counter in order to create a stream of detection times. Both data sets were recorded into binary files on the computer and were analyzed later to provide estimates of the detection rates. In the following each element of the chain is described in more detail.

For the detection of neutrons Westinghouse WL-8073 type *dual range fission chambers* were used [16]. The outer casing of the detector is a cylindrical aluminum tube of height 9.75 in (≈ 248 mm) and diameter 2 in (≈ 51 mm). The filling gas is Argon-Nitrogen mixture at 760 mmHg

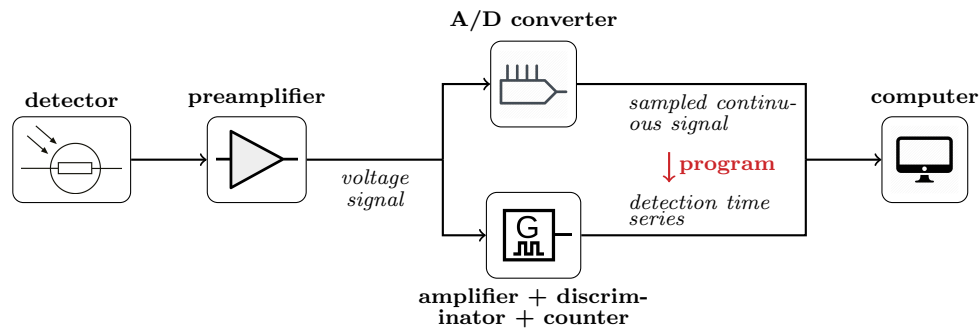


Figure 5.6: The layout of the detection and data acquisition chain.

(≈ 101.3 kPa) pressure. The neutron sensitive fissile deposit consists of U_3O_8 compound enriched to more than 90 % in ^{235}U . The surface density of the deposit is 2 mg/cm^2 whereas its total mass is 1.68 g. No information is available on the structure (number, shape and size) of the electrodes and fissile coatings. This type of detector can be operated both as a counter (for low flux levels) or as an ionization chamber (for high flux levels). The nominal operating voltage is 300 V as a counter and 300 V–1000 V as an ionization chamber. During the measurements the detectors were operated at 300 V. At this value the total thermal neutron sensitivity is $0.7 \text{ counts/neutron/cm}^2$, whereas pulses have an average amplitude of 0.2 mV as well as an average rise time of $0.2 \mu\text{s}$.

The pre-amplifiers were designed and built at the BME Institute of Nuclear Techniques specifically for this measurement [17]. They produce a voltage signal ranging between -1 and 1 V and have a small time constant (compared to the charge collection time of the detector), hence the shapes of the amplified voltage pulses reflect the shapes of the current pulses in the detector itself.

The pre-amplified signal of the detector was sampled, digitized and recorded by a Red Pitaya STEMLab 125-14 multifunction instrument [18]. Each such device has two analogue input channels, hence two instruments were used in the measurements in order to process the signals of all four detectors simultaneously. The device is equipped with a high-performance analog-to-digital (A/D) converter, which provides a maximal sampling rate of 125 million samples per second (corresponding to a 8 ns maximal time resolution) and a fix 14 bit digital resolution. Based on the results of test measurements the time resolution has been set to 40 ns which resolves an average $10 \mu\text{s}$ long pulse (see Figure 5.10) in 250 points. The instrument also comes with an integrated field-programmable gate array (FPGA) unit which stores the digitized signal values in the internal RAM.

A user-written FPGA code was responsible for converting the sampled data into the **time resolved signal format** with the compression algorithm described in Section 3.1, which was then transferred by a C program from the memory of the FPGA to a 32 GB SanDisk Extreme Pro micro SD card. The parameters of the compression algorithm were determined by observing short sections of recorded test signals and took the following values (for their meaning, the reader is referred to Section 3.1): $N_{\text{idle}} = 3$, $N_{\text{head}} = 40$, $N_{\text{tail}} = 250$; the values of $N_{\text{threshold}}$ are given in Table 5.3 for each detector and both measurement configurations. Recall furthermore that the **time resolved signal format** maintains a parameter **baseline** which represents the average value of the background. These have also been determined from the test measurements and are listed in Table 5.4. Every voltage value presented hereafter will be given with respect to the corresponding baseline.

The last item in the amplifier–discriminator–counter chain was a National Instruments myRIO device which recorded the detection events in a time-stamped format. Although this electronic-chain already produced appropriate data for analysis, a second set of detection times were also

Table 5.3: Threshold values applied to discriminate the background fluctuation from the useful parts of the signals.

detector	threshold (mV)	
	Cf	Cf+U
A	65.8	66.2
B	70.4	71.4
C	61.4	65.8
D	70.8	71.0

Table 5.4: Baselines of the detector signals in the two measurement configurations.

detector	baseline (mV)	
	Cf	Cf+U
A	36.7	37.0
B	7.4	7.5
C	30.1	30.0
D	10.5	10.5

created by post-processing the recorded continuous signals using a program. The program implemented a simple integral discriminator logic: given a threshold value, it scans through the continuous signals and determines the times of level crossings. To reduce the number of false counts generated by the electronic noise, the recorded signals have been smoothed using a moving average algorithm before submitting them to the program. The estimation of the detection rates with the pulse counting approach has been performed using both sets of detection times. As we shall see later, the detection rates obtained from this second set show a better agreement with values obtained from the analysis of continuous signals.

The relatively low value of the detection rates predicted by the preliminary simulations (see Table 5.2) suggests that a rather long measurement time (lasting several hours) is required to achieve good statistics, especially in the case of the doubles rates. For this reason, a 14 hour-long measurement was performed in both configurations.

5.4 The characteristics of the recorded continuous signals

In order to gain additional information that might help interpret the measurement data, the characteristics of the pre-amplified detector signals have been investigated. A quick inspection of the signals revealed that it is mainly comprised of fluctuating background (stored in compressed form), while the occasionally occurring uncompressed sections mostly contain a single pulse. Some examples of the recorded pulses are shown in Figure 5.7. The two pulses in the first row are likely been induced by neutrons, since their amplitudes are relatively large. On the other hand, the pulses in the second row have smaller amplitudes and different shapes, hence they might be induced by particles other than neutrons, most likely by α particles from the fissile deposit.

A discrimination against these small amplitude parasitic pulses was clearly necessary when the detection times were derived from the recorded continuous signals by the software. But it was found that they also had to be disregarded to obtain a correct estimate for the average (neutron) pulse in Section 5.5.2. In order to find an appropriate threshold level for the discrimination,

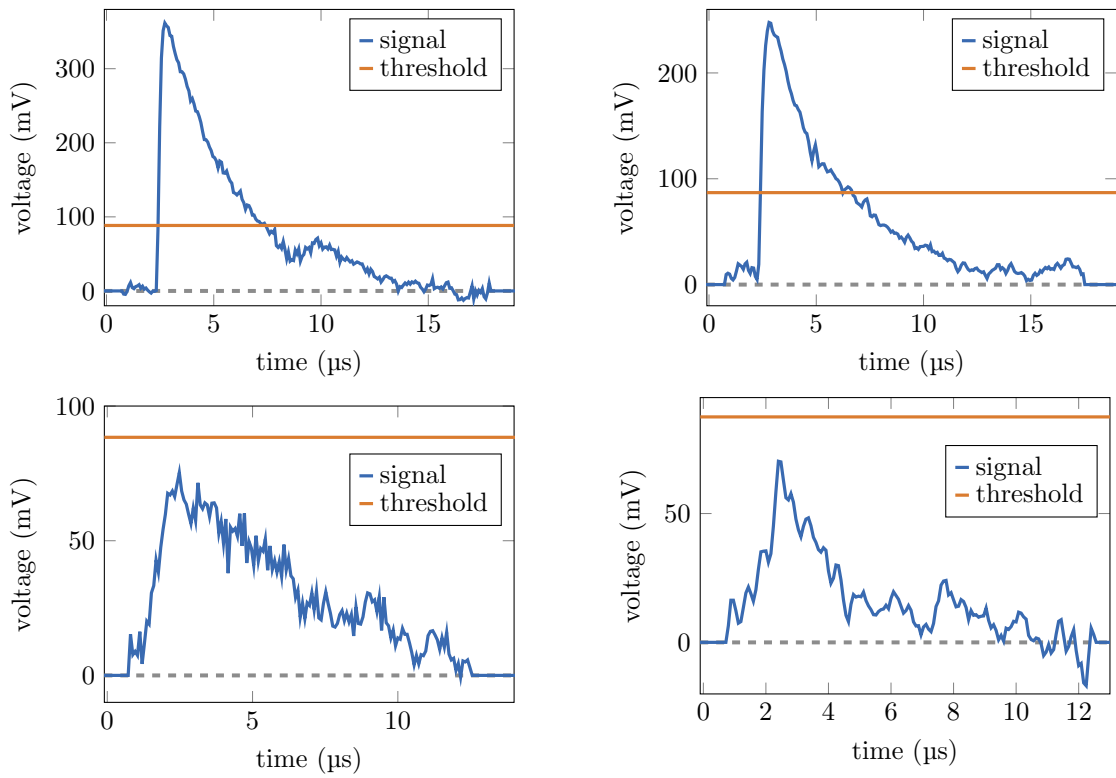


Figure 5.7: Examples of recorded pulses. The orange lines represent the threshold values that were used to discriminate against non-neutron pulses when calculating the average neutron induced pulse.

the pulse height distributions of the recorded signals was calculated. Figure 5.8 shows them in the Cf configuration; they are very similar in the Cf+U configuration. One can see that the majority of pulses have small amplitudes in the range of 70 mV–80 mV, while only few reach a 200 mV height. The smallest observable amplitude is determined by the other type of threshold value used for recording the signal (see Table 5.3). The threshold values for discrimination were chosen to fall into the inflection point of the distribution (except for detector D, where there was none); they are marked by vertical dashed lines in Figure 5.8 and listed in Table 5.5 for all four detectors in both configurations.

Finally, we note that the signal of detector D seemed to contain much more electronic noise than the signals of other detectors. Despite the smoothing applied before determining the times of level crossings, we shall see in Section 5.6 that this noise creates a noticeable amount of false counts.

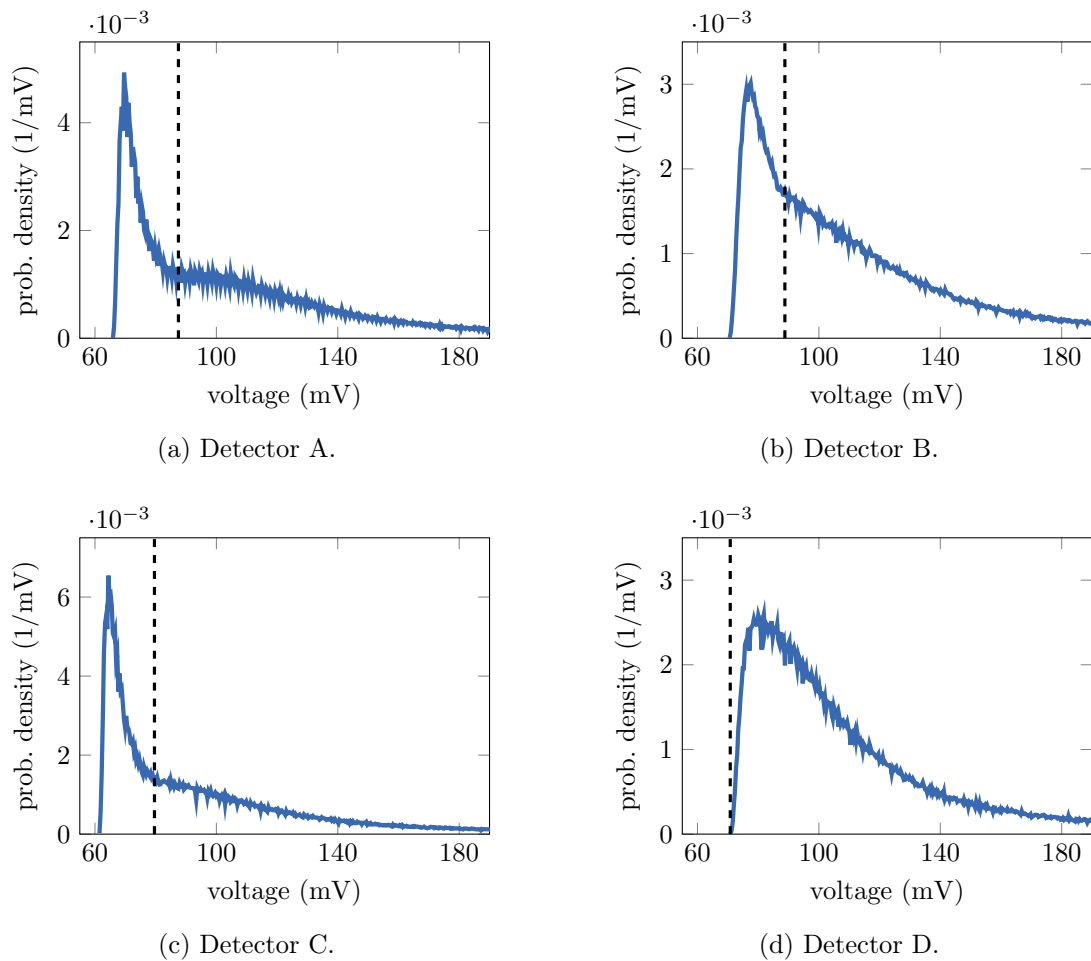


Figure 5.8: The pulse height distribution observed in the signals of detectors A, B, C and D in the Cf measurement configuration. The dashed lines represent the threshold values used to discriminate against non-neutron pulses.

5.5 The estimation of calibration factors

In traditional multiplicity counting, the measured doubles and triples rates (see Equation (2.8)) include the doubles and triples gate fraction factors, f_d and f_t . In the new version of multiplicity

Table 5.5: Threshold values used to discriminate against non-neutron pulses when calculating the average neutron induced pulse.

detector	threshold (mV)	
	Cf	Cf+U
A	87.5	87.2
B	88.8	93.6
C	79.6	86.9
D	70.8	71.0

counting, the measured moments of the signals (see Equations (2.9)–(2.12)) are proportional to different powers of $\langle a \rangle I$, the area under a neutron impulse. Therefore, to be able to compare the results obtained by the two approaches of multiplicity counting, these factors need to be determined by calibration, then the measured quantities need to be converted to the true values of the detection rates.

5.5.1 The gate factors

Instead of the known procedures [4], a semi-empirical approach was chosen to estimate the doubles and triples gate factors. Assuming an exponentially distributed die-away time, they can be written [4] as $f_d = f$ and $f_t = f^2$, where f is given by the expression

$$f = e^{-\tau_{\text{pre}}/\theta} (1 - e^{-\tau_{\text{gate}}/\theta}). \tag{5.1}$$

Here θ is the scale parameter of the exponential distribution, τ_{gate} is the width of the counting gate, whereas τ_{pre} is the so-called predelay, the time between receiving a trigger count and opening the gate [4]. These last two quantities are parameters of the multiplicity counter and are chosen freely; we used the values given in Section 5.6. On the other hand, the scale parameter θ is a property of the experimental set-up which is, however, a-priori unknown. Nevertheless, it is well known that the die-away time scale parameter appears in the mathematical expression of the Rossi-alpha distribution, which characterizes the covariance function of the detector counts [4]. If we instead use its continuous equivalent, the covariance-function of the voltage signals, and we assume a simple exponentially decaying pulse shape with time parameter θ_{pulse} , then, based on the results presented in Reference [3]), one can show that the cross-covariance function of two signals takes the form:

$$\text{Cov}(s) = c \left(\theta e^{-|s|/\theta} - \theta_{\text{pulse}} e^{-|s|/\theta_{\text{pulse}}} \right), \tag{5.2}$$

where c is some constant. By fitting a function of the form (5.2) to a measured cross covariance function of two detector signals, θ can be determined and can be inserted into Equation (5.1) to give an estimate for f which then can be used to calculate the doubles and triples gate factors f_d and f_t . An example of such a fitted covariance function can be seen in Figure 5.9. The values of θ and f obtained for the detector pairs A–B and C–D in both measurement configurations are listed in Table 5.6.

5.5.2 The integral of a neutron induced pulse

The theoretical model, summarized in Section 2.3 assumes that every pulse induced by neutrons has an identical shape (although their amplitudes vary). However, as the examples seen in

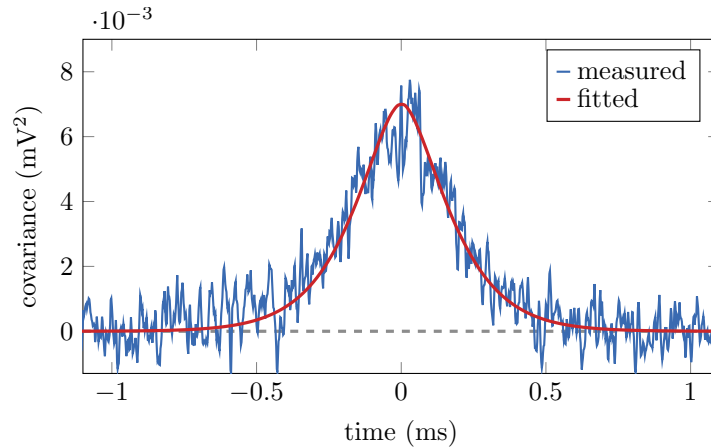


Figure 5.9: Illustration of fitting a function of the form (5.2) to the measured cross covariance function of two detector signals.

Table 5.6: The values of the die-away time parameter θ and the doubles gate fraction ($f_d = f$) obtained from the measured cross covariance functions of detector signals.

detector pair	θ (μs)		f (-)	
	Cf	Cf+U	Cf	Cf+U
A-B	176.26	108.66	0.945	0.912
C-D	109.87	119.51	0.913	0.920

Figure 5.7 testify, the shape of each pulse is unique. For this reason, to provide an estimate of the pulse integral $\langle a \rangle I$, a simple procedure has been designed and implemented.

The procedure relies on the earlier observation, that pulses in the recorded signals are mostly separated i.e. they do not overlap and consists of the following three steps. First, the signals were smoothed using a simple moving average algorithm. Then a program scanned through each signal and calculated the point-by-point average of recorded sections (which likely contain a single pulse). It is crucial, however, that only neutron induced pulses get averaged and pulses induced by other particles (mostly by α particles in our case) are omitted. To achieve this, a threshold value has also been provided to the program as an input parameter and only sections in which the signal reaches the threshold were selected for averaging. Figure 5.10 shows the average neutron pulses determined for all four detectors in the Cf measurement configuration; the results are very similar in the configuration Cf+U. As threshold, the values listed in Table 5.5 were used. Finally, once the average neutron induced pulses have been determined, their integrals could easily be calculated using a numerical scheme such as the trapezoid rule. The values obtained for each detector in both measurement configurations are listed in Table 5.7.

5.6 Estimation of the detection rates

To provide estimates of the detection rates based on the traditional pulse counting approach, a program implementing the logic of a multiplicity shift register (see Reference [4]) was written and used to analyze the detection time series obtained both from the National Instrument myRIO device as well as from the recorded signals using the software described earlier in Section 5.3. The values of the gate width and the predelay parameters (used by the analysis algorithm) were

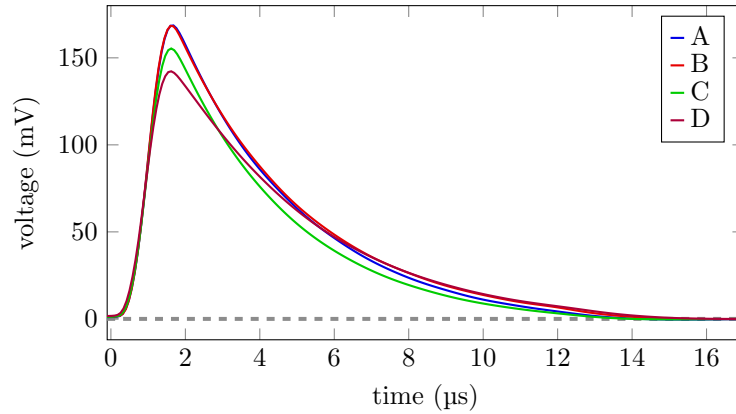


Figure 5.10: Average neutron pulses estimated from the signals of detectors A–D in the Cf measurement configuration.

Table 5.7: Integrals of the average neutron pulses in the two measurement configurations.

detector	average pulse integral (mV s)	
	Cf	Cf + U
A	$4.47 \cdot 10^{-3} \pm 1.8 \cdot 10^{-7}$	$4.49 \cdot 10^{-3} \pm 1.8 \cdot 10^{-7}$
B	$4.60 \cdot 10^{-3} \pm 1.7 \cdot 10^{-7}$	$4.83 \cdot 10^{-3} \pm 1.9 \cdot 10^{-7}$
C	$3.90 \cdot 10^{-3} \pm 1.5 \cdot 10^{-7}$	$4.18 \cdot 10^{-3} \pm 1.7 \cdot 10^{-7}$
D	$4.12 \cdot 10^{-3} \pm 1.4 \cdot 10^{-7}$	$4.18 \cdot 10^{-3} \pm 1.4 \cdot 10^{-7}$

$\theta_{\text{gate}} = 10 \text{ ms}$ and $\theta_{\text{pre}} = 10 \mu\text{s}$. The detection rates output by the analysis program were then corrected with the gate factors (see Section 5.5.1) to be comparable with values obtained from the continuous signals.

The moments of the continuous detector signals were estimated by the `CS analyzer` program described in Section 3.3. During the analysis, the signals were divided into sections of size $N = 200000$; with 48 ns time resolution, this corresponds to a length of $T = 8 \text{ ms}$ in time. From the moments, the detection rates were calculated using the pulse integral values in Table 5.7 with the recovery formulas presented in Section 2.3.

Finally, we note that results will be presented only for the singles and doubles rates. The triples rates could not be estimated for two reasons. First, as the preliminary simulations in Section 5.2 predicted, the detection efficiency was too low to obtain values with acceptable accuracy. The second reason is rooted in the limitations of the data acquisition hardware. Concretely, to estimate the bicovariance function of three signals, they need to be synchronized in time, meaning that corresponding samples were taken from each signal at the same time. This is granted only when they are recorded by the same A/D converter. However, as mentioned in Section 5.3, the Red Pitaya instrument has only two input channels, therefore only two pairs of signals, A–B and C–D, were synchronized. As a consequence, the calculation of the bicovariance function and the triples rate was not possible at all, but even the covariance function (hence the doubles rate) could only be determined for the detector pairs A–B and C–D.

5.6.1 Singles rates

The singles detection rate was estimated for all four detectors separately. The results are summarized in Table 5.8. The third and fourth columns contain the reference singles rates obtained

with pulse counting from the dedicated counter (column *NI myRIO*) as well as from the recorded signals using software (column *program*). In general, the values in these two columns are close to each other. Significant differences can be observed in the case of detector D in both configurations as well as in the case of detector C in the Cf configuration. The larger values observed in the *NI myRIO* column are caused by the noisiness of the signal of detector D that produces false counts (as noted earlier in Section 5.4). The noise is clearly reduced by smoothing the signals as shown by the values presented in column *program*.

The fifth column of Table 5.8, labeled as *original*, contains the singles rates extracted from the mean values of the signals. One can see that these are about 20–30 % larger than the reference values. The deviation is clearly a result of the small amplitude α pulses present in the signal which contribute to the mean value, but which are automatically discriminated against during pulse counting. The solution (measuring the α signal alone, then subtracting its mean value from the mean value of the combined alpha–neutron signal) described in Section 4.5 and demonstrated by simulations cannot be used in this case, since no background measurement is available to us. An alternative approach is followed instead, which is based on the same idea that was used to determine the integral of the neutron induced pulses in Section 5.5.2. Namely, a filtered version of each detector signal is produced by scanning through it and removing sections that contain small amplitude pulses which never cross a predefined threshold value.

The sixth column of Table 5.8, labeled as *filtered*, contains singles rates obtained from such signals created with the threshold values in Table 5.5. Although they are much closer to the reference values than the *original* set, they are still systematically higher by 1–10 %, which indicates that not all parasitic signal components were removed. It is nevertheless rational to expect that when a background measurement is available, the correction can be performed more successfully.

Finally, we note that there is no significant difference between the rates obtained in the two configurations, as it was expected based on the simulation results presented in Section 5.2. We also note that the measured singles rates are 5–15 % smaller than the simulated ones.

Table 5.8: Estimated values of the singles rates obtained from pulse counting and from the mean value of the detector signal.

configuration	detector	singles rate (s^{-1})			
		discrete pulse counting		continuous signal analysis	
		NI myRIO	program	original	filtered
Cf	A	17.019 ± 0.018	17.071 ± 0.018	25.253 ± 0.704	18.282 ± 0.704
	B	17.029 ± 0.018	17.837 ± 0.018	26.714 ± 0.837	19.720 ± 0.838
	C	19.791 ± 0.019	19.759 ± 0.019	31.629 ± 0.920	21.316 ± 0.920
	D	27.391 ± 0.022	21.584 ± 0.020	24.199 ± 0.777	24.198 ± 0.777
Cf+U	A	17.370 ± 0.018	17.475 ± 0.018	26.483 ± 0.806	18.753 ± 0.806
	B	17.627 ± 0.018	16.211 ± 0.018	25.004 ± 0.775	18.047 ± 0.775
	C	19.949 ± 0.019	16.823 ± 0.018	29.881 ± 0.964	18.837 ± 0.964
	D	27.440 ± 0.023	21.793 ± 0.020	24.154 ± 0.800	24.152 ± 0.800

5.6.2 Doubles rates

The doubles detection rate was estimated for the two detector pairs A–B and C–D. The results are shown in Table 5.9, where the columns have the same meaning as in the case of the singles

rate. The doubles rates obtained with pulse counting from the NI myRIO device and from the recorded signals using a program (columns three and four) show a good agreement in the case of the pair A–B. For the pair C–D, however, the difference is significant and has the same reason as before: the noise in the signal of detector D causes false counts in the NI myRIO case, but is reduced by the smoothing in the *program* case. The doubles rates shown in column five, which were recovered from the original detector signals, are systematically larger than the reference values. However, when we again remove the small amplitude pulses from the signals, the obtained detection rates become identical with the reference values within statistical uncertainty, as it can be observed in the sixth column.

The explanation of this phenomenon is less obvious than in the case of the singles rate. Recall that the simulation results of Section 4.5 showed that the doubles estimate is insensitive to the presence of parasitic signal components when they are detection in a Poisson process. Although one would expect the α -background of the fission chamber to be Poissonian, the difference observed between the fifth and sixth columns of the Table observed effect of Table 5.9 might indicate that this is not the case or there are other parasitic components in the signal from other sources as well. A more thorough investigation of this phenomenon will be the topic of a future research activity.

Table 5.9: Estimated values of the doubles rates.

configuration	detector	doubles rate (s ⁻¹)			
		discrete pulse counting		continuous signal analysis	
		NI myRIO	program	original	filtered
Cf	A–B	0.319 ± 0.018	0.291 ± 0.019	0.432 ± 0.009	0.305 ± 0.006
	C–D	0.540 ± 0.027	0.451 ± 0.023	0.428 ± 0.009	0.420 ± 0.008
Cf+U	A–B	0.304 ± 0.020	0.309 ± 0.019	0.433 ± 0.009	0.304 ± 0.007
	C–D	0.538 ± 0.028	0.383 ± 0.022	0.467 ± 0.011	0.376 ± 0.008

Chapter 6

Conclusions

In Section 4 a computational study was performed in order to assess how different factors affect the detection rates recovered from the continuous signals. Most statements concern only the singles and doubles detection rates, since the triples rates could not be obtained with acceptable accuracy.

From all the parameters that were taken into account, the detection efficiency appears to have the most significant influence of the precision of the method: with increasing detection efficiency, the relative error of the estimation decreases rapidly. This suggests that maximizing the detection efficiency should be a priority in practical applications. The second most important parameter has been the measurement time. Although the singles estimate reach a low uncertainty rapidly, the convergence of the doubles rate seemed slow compared to the traditional method, and the triples rate did not reach an acceptable level of uncertainty even at very long measurement times. This topic will be addressed in future research.

Other parameters investigated have either small or negligible influence on the recovered detection rates. Among these, the only considerable bias is the one introduced by a parasitic signal component to the singles rate estimate. Nevertheless, this effect can easily be corrected for by a simple background measurement, as suggested in Section 4.5. No such compensation is required for the doubles rates as it is not affected by the presence of parasitic pulses. Both the singles and doubles rates appear to be insensitive to a Gaussian white noise present in the signal. Finally, it was found that the newly proposed method of multiplicity counting is able to produce correct values for the singles and doubles rates over a wide range of the sample emission intensity; in contrast, the traditional pulse counting approach underestimates the true detection rates at large intensities due to the overlapping of pulses.

Section 5 reported on experimental activities for demonstrating the practical use of the method. A measurement set-up, containing four fission chambers, a ^{252}Cf source and ^{235}U plates, has been designed and built at the KUCA facility of the Kyoto University Institute for Integrated Radiation and Nuclear Science (KURNS). Monte Carlo simulations were performed to optimize the arrangement of the elements of the set-up. An FPGA based fast data acquisition system was assembled to record the voltage signals of the detectors with 8 ns time resolution. The appropriate moments of the signals were estimated and the singles and doubles detection rates were calculated. The triples rates could not be estimated due to the low detection efficiency of the measurement set-up. To serve as a reference, the detection rates were estimated with a traditional pulse counting approach as well. By comparing the results, it has been shown that the new method is able to recover the singles and doubles rates from the signals.

Bibliography

- [1] I. Pázsit, L. Pál, and L. Nagy, “Multiplicity counting from fission chamber signals in the current mode,” *Nuclear Instruments and Methods in Physics Research Section A: Accelerators, Spectrometers, Detectors and Associated Equipment*, vol. 839, pp. 92–101, 2016.
- [2] L. Nagy, I. Pázsit, and L. Pál, “Multiplicity counting from fission detector signals with time delay effects,” *Nuclear Instruments and Methods in Physics Research Section A: Accelerators, Spectrometers, Detectors and Associated Equipment*, vol. 884, pp. 119–127, 2018.
- [3] L. Nagy, I. Pázsit, and L. Pál, “Two- and three-point (in time) statistics of fission chamber signals for multiplicity counting with thermal neutrons,” *Nuclear Instruments and Methods in Physics Research Section A: Accelerators, Spectrometers, Detectors and Associated Equipment*, vol. 929, pp. 148–155, 2019.
- [4] N. Ensslin, W. C. Harker, M. S. Krick, D. G. Langner, M. M. Pickrell, and J. E. Stewart, “Application guide to neutron multiplicity counting,” *Los Alamos Report LA-13422-M*, 1998.
- [5] I. Pázsit and L. Pál, *Neutron Fluctuations: a Treatise on the Physics of Branching Processes*. New York, London, Tokyo: Elsevier, 1st ed., 2008.
- [6] L. Pál, I. Pázsit, and Zs. Elter, “Comments on the stochastic characteristics of fission chamber signals,” *Nuclear Instruments and Methods in Physics Research Section A: Accelerators, Spectrometers, Detectors and Associated Equipment*, vol. 763, no. 0, pp. 44–52, 2014.
- [7] K. Böhnel, “The effect of multiplication on the quantitative determination of spontaneously fissioning isotopes by neutron correlation analysis,” *Nuclear Science and Engineering*, vol. 90, no. 1, pp. 75–82, 1985.
- [8] I. Pázsit, A. Enqvist, and L. Pál, “A note on the multiplicity expressions in nuclear safeguards,” *Nuclear Instruments and Methods in Physics Research Section A: Accelerators, Spectrometers, Detectors and Associated Equipment*, vol. 603, no. 3, pp. 541–544, 2009.
- [9] A. Papoulis and H. Saunders, *Probability, random variables and stochastic processes*. McGraw-Hill Book Co., 1989.
- [10] D. Reilly, N. Ensslin, H. Smith Jr, and S. Kreiner, *Passive nondestructive assay of nuclear materials*, ch. ”The Origin of Neutron Radiation”. Washington DC, United States: Nuclear Regulatory Commission, Office of Nuclear Regulatory Research; Los Alamos National Lab., NM (United States), 1991.
- [11] G. F. Knoll, *Radiation detection and measurement*. John Wiley & Sons, 2010.
- [12] Zs. Elter, G. de Izarra, P. Filliatre, C. Jammes, and I. Pázsit, “Performance of higher order Campbell methods, Part II: calibration and experimental application,” *Nuclear Instruments*

and Methods in Physics Research Section A: Accelerators, Spectrometers, Detectors and Associated Equipment, vol. 835, pp. 86–93, 2016.

- [13] I. Lux and A. Baranyai, “Higher order campbell techniques for neutron flux measurement: I. theory,” *Nuclear Instruments and Methods in Physics Research*, vol. 202, no. 3, pp. 469–475, 1982.
- [14] C. H. Pyeon, “Experimental benchmarks for accelerator-driven system (ADS) at kyoto university critical assembly,” Tech. Rep. KURRI-TR-444, Research Reactor Institute, Kyoto University, 2013.
- [15] D. B. Pelowitz, “MCNPX user’s manual version 2.7. 0-LA-CP-11-00438,” *Los Alamos National Laboratory*, 2011.
- [16] Westinghouse Electric Corporation, Electronic Tube Division, Elmira, New York, *Westinghouse Dual Range Fission Chamber Type 8073 Data Sheet*, May 15, 1961. URL: <https://frank.pocnet.net/sheets/201/8/8073.pdf> (accessed: March, 2021).
- [17] G. Klujber, I. Barth, and M. Szieberth, “Construction of a data acquisition system for recording the continuous signals of fission chambers (in Hungarian),” Tech. Rep. BME-NTI-887/2019, Institute of Nuclear Techniques, Budapest University of Technology and Economics, 2019.
- [18] Red Pitaya d.d., Velika pot 22, 5250 Solkan, Slovenia, *Red Pitaya Stemplab Board – Data Sheet*. URL: <https://www.redpitaya.com/f130/red-pitaya-stemplab-board>, accessed: March, 2021.